

On the Optimal MMSE Channel Estimation for One-Bit Quantized MIMO Systems

Minhua Ding, Italo Atzeni, *Member, IEEE*,

Antti Tölli, *Senior Member, IEEE*, and A. Lee Swindlehurst, *Fellow, IEEE*.

Abstract—This paper focuses on the minimum mean squared error (MMSE) channel estimator for multiple-input multiple-output (MIMO) systems with one-bit quantization at the receiver side. Despite its optimality and significance in estimation theory, the MMSE channel estimator has not been fully investigated in this context due to its general non-linearity and computational complexity. Instead, the typically suboptimal Bussgang linear MMSE (BLMMSE) estimator has been widely adopted. In this work, we develop a new framework to compute the MMSE channel estimator that hinges on computation of the orthant probability of the multivariate normal distribution. Based on this framework, we determine a necessary and sufficient condition for the BLMMSE channel estimator to be optimal and equivalent to the MMSE estimator. Under the assumption of specific channel correlation or pilot symbols, we further utilize the framework to derive analytical expressions for the MMSE channel estimator that are particularly convenient for computation when certain system dimensions become large, thereby enabling a comparison between the BLMMSE and MMSE channel estimators in these cases.

Index Terms—Channel estimation, massive MIMO, minimum mean squared error (MMSE), one-bit quantization, orthant probability.

I. INTRODUCTION

Due to its potential to significantly enhance spectral efficiency and reliability [1]–[3], state-of-the-art wireless networks employ multiple-input multiple-output (MIMO) transceivers with large numbers of antennas, and such systems are envisioned to assume an even more prominent role in future wireless systems [4]. However, deploying transceivers with many antennas motivates study of the use and impact of low-cost, energy-efficient hardware on system performance metrics.

One of the main challenges in implementing a fully digital high-resolution massive MIMO system is the prohibitively high power consumption of the analog-to-digital/digital-to-analog converters (ADCs/DACs), which scales exponentially with the number of resolution bits [5]–[8]. Against this backdrop, there is a large body of literature investigating massive MIMO systems with low-resolution ADCs [6]–[19]. In particular, one-bit quantization for massive MIMO systems has received special attention due to its energy efficiency and

low complexity. The capacity of MIMO channels with one-bit ADCs was investigated in [6] assuming perfect channel state information (CSI) at both the transmitter and the receiver, whereas capacity bounds for one-bit MIMO Gaussian channels with analog combining were studied in [12]. Assuming perfect CSI at the receiver, one-bit MIMO-OFDM detection based on inexact variants of the classical expectation-maximization method was considered in [13].

Most massive MIMO systems require CSI to facilitate beamforming design. Channel estimation based on one-bit quantized measurements is thus of great importance [7], [14]–[17], [19]. In this respect, an approach based on maximum likelihood (ML) was used for channel estimation in connection with near-ML data detection in [14], while the Cramér-Rao performance bounds for channel estimation in one-bit quantized massive MIMO were studied in [15]. Channel estimation from one-bit quantized measurements with an unknown threshold was considered in [16]. The Bussgang linear minimum mean squared error (BLMMSE) channel estimator proposed in [7] elegantly used the second-order statistics of one-bit quantized signals [20], [21], and its linear structure inspired subsequent signal processing methods applied to, e.g., data detection [17], [18] and precoding design [22], [23].

Despite its optimality in terms of mean squared error (MSE) and its significance in estimation theory, the minimum MSE (MMSE) channel estimator, also known as the conditional mean estimator (CME) [19], [24], [25, p. 17, (2.36)], has not been well investigated for one-bit quantized MIMO systems. The authors of [19] established the equivalence between the BLMMSE and the optimal MMSE channel estimates in single-input single-output (SISO) systems with one pilot symbol, as well as in noiseless SISO systems with multiple (specifically chosen) pilot symbols. However, some questions remain unanswered regarding the CME for one-bit quantized MIMO systems. Furthermore, explicit computation of the MMSE estimate still appears elusive due to the required multi-dimensional integration involving a multivariate normal (MVN) distribution [19], [24].

In this work, we aim at providing further results on the optimal MMSE channel estimator for MIMO systems with one-bit ADCs. We consider a point-to-point MIMO system to focus on the fundamental estimation problem, although our results can be framed for a multi-user uplink system with single-antenna users and a multi-antenna base station (BS). Despite the complexity of the estimation problem, we obtain several new results, which are summarized as follows.

- 1) We first develop a general framework for computing the

M. Ding, I. Atzeni, and A. Tölli are with the Centre for Wireless Communications, University of Oulu, Finland (e-mails: {minhua.ding, italo.atzeni, antti.tolli}@oulu.fi). A. L. Swindlehurst is with the Center for Pervasive Communications and Computing, University of California, Irvine, CA, USA (e-mail: swindle@uci.edu). This work was supported by the Research Council of Finland (318927 6G Flagship, 336449 Profi6, 348396 HIGH-6G, and 357504 EETCAMD) and by the U. S. National Science Foundation (CCF-2225575)

MMSE channel estimate, which relies on computation of the *orthant probability* of an MVN distribution. The Gaussian orthant probability has been investigated in the literature [26]–[31] and used in various engineering fields [32], [33]. Therefore, our framework connects MMSE estimation to a wider class of problems.

- 2) Based on the above framework, we determine a necessary and sufficient condition for the equivalence of the BLMMSE and MMSE channel estimates in one-bit quantized MIMO systems. Moreover, we examine specific cases where this equivalence holds.
- 3) The simplest case where the BLMMSE channel estimate becomes suboptimal is identified to correspond to a single-input multiple-output (SIMO) system with real-valued full channel correlation among three receive antennas. For this case, we present a closed-form expression of the optimal (non-linear) MMSE estimate.
- 4) We derive an expression for the MMSE channel estimate for SIMO channels with a single pilot symbol assuming real-valued equal correlation among all the receive antennas. In addition, we derive an expression for the optimal MMSE channel estimate for SISO channels or spatially white SIMO channels with multiple real-valued pilot symbols. These formulas only require one-dimensional integration and can thus be efficiently computed using common software when either the number of receive antennas or the number of pilot symbols becomes large.

Outline. The rest of the paper is organized as follows. Section II describes the system model and the goal of our investigation. Section III develops the framework for computing the MMSE channel estimate in one-bit quantized MIMO systems. After providing background on the Gaussian orthant probability in Section IV, the condition for the optimality of the BLMMSE channel estimate is presented in Section V. Various results on the MMSE channel estimate are discussed in Section VI, whereas simulation results are provided in Section VII. Finally, Section VIII concludes the paper.

Notation. Lowercase letters, bold lowercase letters, and bold uppercase letters denote scalars, vectors, and matrices, respectively. The quantity x_k represents the k -th element of vector \mathbf{x} and $[\mathbf{X}]_{ik}$ denotes the (i, k) -th element of matrix \mathbf{X} . We let $(\cdot)^*$, $(\cdot)^T$, and $(\cdot)^H$ denote complex conjugate, transpose, and Hermitian transpose, respectively. The $n \times n$ identity matrix is written as \mathbf{I}_n . The operator \otimes represents the Kronecker product, $|\mathbf{X}|$ denotes the determinant of a square matrix \mathbf{X} , $\text{vec}(\cdot)$ denotes vectorization, $\|\mathbf{x}\| = \sqrt{\mathbf{x}^H \mathbf{x}}$, $|x|$ denotes the modulus of x , and $j = \sqrt{-1}$. The sets of real-valued non-negative, real-valued, and complex-valued n -dimensional vectors are denoted by \mathbb{R}_+^n , \mathbb{R}^n , and \mathbb{C}^n , respectively, whereas the sets of real- and complex-valued $m \times n$ matrices are denoted by $\mathbb{R}^{m \times n}$ and $\mathbb{C}^{m \times n}$, respectively. Real-valued and circularly symmetric complex-valued MVN distributions with mean $\boldsymbol{\mu}$ and covariance matrix $\boldsymbol{\Sigma}$ are respectively indicated by $\mathcal{N}(\boldsymbol{\mu}, \boldsymbol{\Sigma})$ and $\mathcal{CN}(\boldsymbol{\mu}, \boldsymbol{\Sigma})$. The operators $\mathbb{E}(\cdot)$ and $\text{Pr}(\cdot)$ represent statistical expectation and probability, respectively. In addition, $[z_k]_{k=1}^m$ represents the vector with

elements z_1, \dots, z_m , $\text{diag}(\mathbf{z})$ is a diagonal matrix with the elements of \mathbf{z} on its diagonal, $\text{diag}(\mathbf{X})$ is the diagonal matrix formed using the diagonal elements of the arbitrary square matrix \mathbf{X} , and $\text{DIAG}(\mathbf{Y}_1, \dots, \mathbf{Y}_n)$ is a block-diagonal matrix with $\mathbf{Y}_1, \dots, \mathbf{Y}_n$ representing the blocks along the diagonal.

II. SYSTEM MODEL AND PROBLEM STATEMENT

A. System Model

Consider a general MIMO system with N_T transmit antennas and N_R receive antennas. Assume slow flat Rayleigh fading, and let $\mathbf{H} \in \mathbb{C}^{N_R \times N_T}$ denote the channel matrix between the transmitter and the receiver.

For channel estimation, τ pilot symbols per antenna are transmitted, which are collectively denoted by $\mathbf{S}^T = [\mathbf{s}_1 \dots \mathbf{s}_\tau] \in \mathbb{C}^{N_T \times \tau}$. We define the received signal (at the input of the ADCs) as

$$\mathbf{B} = \mathbf{H}\mathbf{S}^T + \mathbf{N} = [\mathbf{b}_1 \dots \mathbf{b}_\tau] \in \mathbb{C}^{N_R \times \tau}, \quad (1)$$

where $\mathbf{N} = [\mathbf{n}_1 \dots \mathbf{n}_\tau] \in \mathbb{C}^{N_R \times \tau}$ represents the noise matrix. Furthermore, we introduce

$$\mathbf{b} = \text{vec}(\mathbf{B}) = (\mathbf{S} \otimes \mathbf{I}_{N_R})\mathbf{h} + \mathbf{n} = \mathbf{A}\mathbf{h} + \mathbf{n} \in \mathbb{C}^{\tau N_R}, \quad (2)$$

with $\mathbf{h} = \text{vec}(\mathbf{H}) \in \mathbb{C}^{N_T N_R}$, $\mathbf{n} = \text{vec}(\mathbf{N}) \in \mathbb{C}^{\tau N_R}$, and

$$\mathbf{A} = \mathbf{S} \otimes \mathbf{I}_{N_R} \in \mathbb{C}^{(\tau N_R) \times (N_T N_R)}. \quad (3)$$

Based on the channel assumption, $\mathbf{h} \sim \mathcal{CN}(\mathbf{0}, \boldsymbol{\Sigma})$, where $\boldsymbol{\Sigma}$ represents the $(N_T N_R) \times (N_T N_R)$ channel covariance matrix, and its joint probability density function (pdf) is given by

$$p(\mathbf{h}) = \frac{1}{\pi^{N_T N_R} |\boldsymbol{\Sigma}|} \exp\{-\mathbf{h}^H \boldsymbol{\Sigma}^{-1} \mathbf{h}\}. \quad (4)$$

The additive Gaussian noise samples are assumed to be spatially and temporally white, i.e., $\mathbf{n} \sim \mathcal{CN}(\mathbf{0}, \sigma^2 \mathbf{I}_{\tau N_R})$.

We denote the element-wise memoryless one-bit quantization operation as

$$\mathcal{Q}_{\text{1bit}}(\cdot) = \text{sgn}(\Re(\cdot)) + j \text{sgn}(\Im(\cdot)), \quad (5)$$

where $\text{sgn}(\cdot)$ denotes the sign function and $\Re(\cdot)$ (resp. $\Im(\cdot)$) represents the real (resp. imaginary) part. The quantized received signal (at the output of the ADCs) is given by

$$\mathbf{r} = \mathcal{Q}_{\text{1bit}}(\mathbf{b}) \in \mathbb{C}^{\tau N_R}. \quad (6)$$

B. Problem Statement

Our goal is two-fold.

- 1) Based on the quantized output \mathbf{r} , the MMSE estimate of \mathbf{h} is given by $\hat{\mathbf{h}}_{\text{MMSE}} = \mathbb{E}(\mathbf{h}|\mathbf{r}) = \int_{\mathbb{C}^{N_T N_R}} \mathbf{h} p(\mathbf{h}|\mathbf{r}) d\mathbf{h}$, with $p(\mathbf{h}|\mathbf{r}) = \text{Pr}(\mathbf{r}|\mathbf{h})p(\mathbf{h}) / \text{Pr}(\mathbf{r})$. Therefore,

$$\hat{\mathbf{h}}_{\text{MMSE}} = \frac{\int_{\mathbb{C}^{N_T N_R}} \mathbf{h} \text{Pr}(\mathbf{r}|\mathbf{h})p(\mathbf{h}) d\mathbf{h}}{\text{Pr}(\mathbf{r})}, \quad (7)$$

with

$$\text{Pr}(\mathbf{r}) = \int_{\mathbb{C}^{N_T N_R}} \text{Pr}(\mathbf{r}|\mathbf{h})p(\mathbf{h}) d\mathbf{h}. \quad (8)$$

Since there are no explicit details in the literature on how to compute (7), we first develop a novel framework for

its computation, and then we determine a necessary and sufficient condition under which the MMSE estimate is linear, i.e., a necessary and sufficient condition for the BLMMSE channel estimator to be MSE-optimal.

- 2) We further identify the simplest case where the MMSE estimate admits a closed-form solution. Despite the generic complexity of computing (7) [19], under specific assumptions on the channel correlation or pilot symbols, we aim at obtaining computationally efficient analytical expressions for $\hat{\mathbf{h}}_{\text{MMSE}}$ that facilitate insight into its performance when certain system dimensions, i.e., the number of receive antennas or the number of pilot symbols, become large.

III. A FRAMEWORK FOR ONE-BIT MMSE CHANNEL ESTIMATION

Our goal in this section is to examine the structure of the MMSE channel estimator with one-bit observations and reformulate the corresponding conditional mean expression into a form that involves the Gaussian orthant probability. This probability will then be exploited in the following section to find a condition that can be used to determine the optimality of the BLMMSE estimator.

Recall (2) and (5)–(6), and let $\mathbf{r} = \mathbf{r}_R + j\mathbf{r}_I$, with

$$\mathbf{r}_R = \Re(\mathbf{r}) = \text{sgn}(\Re(\mathbf{b})), \quad \mathbf{r}_I = \Im(\mathbf{r}) = \text{sgn}(\Im(\mathbf{b})). \quad (9)$$

Then, $r_{R,k} = \Re(r_k)$ and $r_{I,k} = \Im(r_k)$, with $r_{R,k}, r_{I,k} \in \{\pm 1\}$, for $k = 1, \dots, \tau N_R$. Correspondingly, we have

$$\begin{aligned} r_k &= r_{R,k} + jr_{I,k} = \text{sgn}(\Re(b_k)) + j\text{sgn}(\Im(b_k)) \\ &= \text{sgn}(\Re(\mathbf{a}_k^T \mathbf{h}) + \Re(n_k)) + j\text{sgn}(\Im(\mathbf{a}_k^T \mathbf{h}) + \Im(n_k)), \end{aligned} \quad (10)$$

where \mathbf{a}_k^T denotes the k -th row of \mathbf{A} , $\Re(n_k)$ and $\Im(n_k)$ are independent and identically distributed (i.i.d.) $\mathcal{N}(0, \frac{\sigma^2}{2})$ random variables, and

$$(\Re(\mathbf{a}_k^T \mathbf{h}))^2 + (\Im(\mathbf{a}_k^T \mathbf{h}))^2 = \mathbf{h}^H \mathbf{a}_k \mathbf{a}_k^T \mathbf{h}, \quad (12)$$

for $k = 1, \dots, \tau N_R$. It can be readily shown that

$$\Pr(r_{R,k} | \mathbf{h}) = \int_0^\infty \frac{\exp\left\{-\frac{1}{\sigma^2} (x_k - r_{R,k} \Re(\mathbf{a}_k^T \mathbf{h}))^2\right\}}{\sqrt{\pi\sigma^2}} dx_k, \quad (13)$$

$$\Pr(r_{I,k} | \mathbf{h}) = \int_0^\infty \frac{\exp\left\{-\frac{1}{\sigma^2} (y_k - r_{I,k} \Im(\mathbf{a}_k^T \mathbf{h}))^2\right\}}{\sqrt{\pi\sigma^2}} dy_k. \quad (14)$$

Based on the distribution of the noise, we have

$$\Pr(r_k | \mathbf{h}) = \Pr(r_{R,k} | \mathbf{h}) \Pr(r_{I,k} | \mathbf{h}), \quad (15)$$

$k = 1, \dots, \tau N_R$, and thus

$$\begin{aligned} \Pr(\mathbf{r} | \mathbf{h}) &= \prod_{k=1}^{\tau N_R} \Pr(r_k | \mathbf{h}) \\ &= \int_{\mathbb{R}_+^{\tau N_R}} \int_{\mathbb{R}_+^{\tau N_R}} \frac{e^{-\sum_{k=1}^{\tau N_R} \frac{(x_k - r_{R,k} \Re(\mathbf{a}_k^T \mathbf{h}))^2 + (y_k - r_{I,k} \Im(\mathbf{a}_k^T \mathbf{h}))^2}{\sigma^2}}}{(\pi\sigma^2)^{\tau N_R}} dx dy, \end{aligned} \quad (17)$$

with

$$\mathbf{x} = [x_1 \dots x_{\tau N_R}]^T, \quad \mathbf{y} = [y_1 \dots y_{\tau N_R}]^T. \quad (18)$$

Define

$$\Lambda_R = \text{diag}(\mathbf{r}_R), \quad \Lambda_I = \text{diag}(\mathbf{r}_I), \quad (19)$$

and note that $\Lambda_R \Lambda_R = \Lambda_I \Lambda_I = \mathbf{I}_{\tau N_R}$. Then, (17) is equivalent to

$$\Pr(\mathbf{r} | \mathbf{h}) = \int_{\mathbb{R}_+^{\tau N_R}} \int_{\mathbb{R}_+^{\tau N_R}} \frac{\exp\left\{-\frac{\|\Lambda_R \mathbf{x} + j\Lambda_I \mathbf{y} - \mathbf{A}\mathbf{h}\|^2}{\sigma^2}\right\}}{(\pi\sigma^2)^{\tau N_R}} dx dy. \quad (20)$$

The covariance matrix of \mathbf{b} in (2) is given by

$$\Omega_b = \mathbf{A}\Sigma\mathbf{A}^H + \sigma^2\mathbf{I}_{\tau N_R} \in \mathbb{C}^{(\tau N_R) \times (\tau N_R)}. \quad (21)$$

For subsequent derivation, let $\Theta = (\Sigma^{-1} + \frac{1}{\sigma^2}\mathbf{A}^H\mathbf{A})^{-1}$ and let $\boldsymbol{\mu}_h = \frac{1}{\sigma^2}\Theta\mathbf{A}^H(\Lambda_R\mathbf{x} + j\Lambda_I\mathbf{y})$. Using the matrix inversion identity [34], we have $\frac{1}{\sigma^2}\Theta\mathbf{A}^H = \Sigma\mathbf{A}^H\Omega_b^{-1}$ and thus, $\boldsymbol{\mu}_h = \Sigma\mathbf{A}^H\Omega_b^{-1}(\Lambda_R\mathbf{x} + j\Lambda_I\mathbf{y})$. Based on (4) and (20), it can be shown that (8) is given by

$$\begin{aligned} \Pr(\mathbf{r}) &= \int_{\mathbb{C}^{N_T N_R}} \Pr(\mathbf{r} | \mathbf{h}) \left\{ \frac{\exp\{-\mathbf{h}^H \Sigma^{-1} \mathbf{h}\}}{\pi^{N_T N_R} |\Sigma|} \right\} d\mathbf{h} \\ &= \int_{\mathbb{R}_+^{\tau N_R}} \int_{\mathbb{R}_+^{\tau N_R}} \frac{e^{-\frac{1}{\sigma^2} \|\Lambda_R \mathbf{x} + j\Lambda_I \mathbf{y}\|^2} e^{\boldsymbol{\mu}_h^H \Theta^{-1} \boldsymbol{\mu}_h}}{\pi^{\tau N_R} |\Omega_b|} dx dy, \end{aligned} \quad (22)$$

where we have used the fact that $\mathcal{CN}(\boldsymbol{\mu}_h, \Theta)$ integrates to one over its entire support. Further algebraic manipulations yield

$$\begin{aligned} \Pr(\mathbf{r}) &= \int_{\mathbb{R}_+^{\tau N_R}} \int_{\mathbb{R}_+^{\tau N_R}} \frac{e^{-(\mathbf{x}^T \Lambda_R \mathbf{D}_R \Lambda_R \mathbf{x} + \mathbf{y}^T \Lambda_I \mathbf{D}_R \Lambda_I \mathbf{y} - 2\mathbf{x}^T \Lambda_R \mathbf{D}_I \Lambda_I \mathbf{y})}}{\pi^{\tau N_R} |\Omega_b|} dx dy, \end{aligned} \quad (24)$$

with

$$\mathbf{D}_R = \Re(\Omega_b^{-1}) = \mathbf{D}_R^T \in \mathbb{R}^{(\tau N_R) \times (\tau N_R)}, \quad (25)$$

$$\mathbf{D}_I = \Im(\Omega_b^{-1}) = -\mathbf{D}_I^T \in \mathbb{R}^{(\tau N_R) \times (\tau N_R)}. \quad (26)$$

At this point, (24) can be compactly expressed as

$$\Pr(\mathbf{r}) = \frac{1}{\pi^{\tau N_R} |\Omega_b|} \int_{\mathbb{R}^{2\tau N_R}} \exp\{-\mathbf{z}^T \mathbf{C} \mathbf{z}\} d\mathbf{z}, \quad (27)$$

with

$$\mathbf{C} = \begin{bmatrix} \Lambda_R \mathbf{D}_R \Lambda_R & \Lambda_R \mathbf{D}_I^T \Lambda_I \\ \Lambda_I \mathbf{D}_I \Lambda_R & \Lambda_I \mathbf{D}_R \Lambda_I \end{bmatrix} \in \mathbb{R}^{(2\tau N_R) \times (2\tau N_R)}, \quad (28)$$

$$\mathbf{z} = [\mathbf{x}^T \ \mathbf{y}^T]^T \in \mathbb{R}^{2\tau N_R}. \quad (29)$$

Similarly, the numerator of (7) is given by

$$\begin{aligned} \int_{\mathbb{C}^{N_T N_R}} \mathbf{h} \Pr(\mathbf{r} | \mathbf{h}) p(\mathbf{h}) d\mathbf{h} &= \frac{\Sigma \mathbf{A}^H \Omega_b^{-1} [\Lambda_R \ j\Lambda_I]}{\pi^{\tau N_R} |\Omega_b|} \\ &\cdot \int_{\mathbb{R}_+^{2\tau N_R}} \mathbf{z} e^{-\mathbf{z}^T \mathbf{C} \mathbf{z}} d\mathbf{z}. \end{aligned} \quad (30)$$

Based on (7), (27), and (30), we have

$$\hat{\mathbf{h}}_{\text{MMSE}} = \mathbf{\Sigma} \mathbf{A}^H \mathbf{\Omega}_b^{-1} [\mathbf{\Lambda}_R \ j \mathbf{\Lambda}_I] \left(\frac{\int_{\mathbb{R}_+^{2\tau N_R}} \mathbf{z} e^{-\mathbf{z}^T \mathbf{C} \mathbf{z}} d\mathbf{z}}{\int_{\mathbb{R}_+^{2\tau N_R}} e^{-\mathbf{z}^T \mathbf{C} \mathbf{z}} d\mathbf{z}} \right). \quad (31)$$

Note that the quotient of the integrals in (31) denotes the mean of a truncated MVN distribution with $\mathbb{R}_+^{2\tau N_R}$ as its support. Moreover, since

$$\frac{d}{d\mathbf{z}} \exp \{-\mathbf{z}^T \mathbf{C} \mathbf{z}\} = -2\mathbf{C} \mathbf{z} \exp \{-\mathbf{z}^T \mathbf{C} \mathbf{z}\}, \quad (32)$$

we have

$$\int_{\mathbb{R}_+^{2\tau N_R}} \mathbf{z} \exp \{-\mathbf{z}^T \mathbf{C} \mathbf{z}\} d\mathbf{z} = \frac{1}{2} \mathbf{C}^{-1} \boldsymbol{\alpha}, \quad (33)$$

where the k -th element of $\boldsymbol{\alpha} \in \mathbb{R}^{2\tau N_R}$ is given by

$$\alpha_k = \int_{\mathbb{R}_+^{2\tau N_R - 1}} \exp \{-\mathbf{z}_{-k}^T \mathbf{C}_{-k} \mathbf{z}_{-k}\} d\mathbf{z}_{-k}, \quad (34)$$

with $\mathbf{z}_{-k} = [z_1 \ \dots \ z_{k-1} \ z_{k+1} \ \dots \ z_{2\tau N_R}]^T \in \mathbb{R}^{2\tau N_R - 1}$ and where $\mathbf{C}_{-k} \in \mathbb{R}^{(2\tau N_R - 1) \times (2\tau N_R - 1)}$ is obtained by deleting the k -th row and column of \mathbf{C} . Consequently, (31) is equivalent to

$$\hat{\mathbf{h}}_{\text{MMSE}} = \frac{\mathbf{\Sigma} \mathbf{A}^H \mathbf{\Omega}_b^{-1} [\mathbf{\Lambda}_R \ j \mathbf{\Lambda}_I] \mathbf{C}^{-1} \boldsymbol{\alpha}}{2 \int_{\mathbb{R}_+^{2\tau N_R}} \exp \{-\mathbf{z}^T \mathbf{C} \mathbf{z}\} d\mathbf{z}}. \quad (35)$$

Remark 1. In the expression for $\hat{\mathbf{h}}_{\text{MMSE}}$ used in [19], the quantized outputs (i.e., (9) or (19)) affect the integration limits. In contrast, in (31) and (35), they appear outside the integrals and in the integrands through \mathbf{C} and \mathbf{C}_{-k} , for $k = 1, \dots, 2\tau N_R$, which facilitates linking $\hat{\mathbf{h}}_{\text{MMSE}}$ to the Gaussian orthant probability, as will be shown later.

Remark 2. The diagonal elements of \mathbf{C} are not affected by the quantized output. Each off-diagonal element of \mathbf{C} is affected by exactly two different elements from $[\mathbf{r}_R^T \ \mathbf{r}_I^T]^T$. The same comments also apply to \mathbf{C}_{-k} , for $k = 1, \dots, 2\tau N_R$. These observations are instrumental for deriving simplified but equivalent expressions for $\hat{\mathbf{h}}_{\text{MMSE}}$ under specific assumptions on the channel correlation or pilot symbols (see Theorems 3 and 4 in Section VI).

In (35), the expression for $\hat{\mathbf{h}}_{\text{MMSE}}$ is directly related to the orthant probability of the real-valued MVN distribution defined below [26], [32], [33]:

$$\mathcal{P}(\boldsymbol{\Psi}) = \frac{1}{(2\pi)^{\frac{L}{2}} |\boldsymbol{\Psi}|^{\frac{1}{2}}} \int_{\mathbb{R}_+^L} \exp \left\{ -\frac{1}{2} \mathbf{u}^T \boldsymbol{\Psi}^{-1} \mathbf{u} \right\} d\mathbf{u}, \quad (36)$$

where $\boldsymbol{\Psi}$ denotes the $L \times L$ covariance matrix in $\mathcal{N}(\mathbf{0}, \boldsymbol{\Psi})$. Using the notation in (36), (34) is equivalently expressed as

$$\alpha_k = (2\pi)^{\frac{2\tau N_R - 1}{2}} \left| \frac{1}{2} \mathbf{C}_{-k}^{-1} \right|^{\frac{1}{2}} \mathcal{P} \left(\frac{1}{2} \mathbf{C}_{-k}^{-1} \right), \quad (37)$$

and the integral in the denominator of (35) is given by

$$\int_{\mathbb{R}_+^{2\tau N_R}} e^{-\mathbf{z}^T \mathbf{C} \mathbf{z}} d\mathbf{z} = (2\pi)^{\tau N_R} \left| \frac{1}{2} \mathbf{C}^{-1} \right|^{\frac{1}{2}} \mathcal{P} \left(\frac{1}{2} \mathbf{C}^{-1} \right). \quad (38)$$

It can also be shown that, for $k = 1, \dots, 2\tau N_R$,

$$|\mathbf{C}_{-k}^{-1}| / |\mathbf{C}^{-1}| = |\mathbf{C}| / |\mathbf{C}_{-k}| = 1 / [\mathbf{C}^{-1}]_{kk}. \quad (39)$$

Based on (37)–(39), (35) is shown to be equivalent to

$$\hat{\mathbf{h}}_{\text{MMSE}} = \frac{\mathbf{\Sigma} \mathbf{A}^H \mathbf{\Omega}_b^{-1} [\mathbf{\Lambda}_R \ j \mathbf{\Lambda}_I] \mathbf{C}^{-1} \left(\widetilde{\text{diag}}(\mathbf{C}^{-1}) \right)^{-\frac{1}{2}} \mathbf{g}}{2\sqrt{\pi} \mathcal{P} \left(\frac{1}{2} \mathbf{C}^{-1} \right)}, \quad (40)$$

where the k -th element of \mathbf{g} is given by

$$g_k = \mathcal{P} \left(\frac{1}{2} \mathbf{C}_{-k}^{-1} \right) \quad (k = 1, \dots, 2\tau N_R). \quad (41)$$

Remark 3. From (3), (28), (31), (35), and (40)–(41), the channel covariance matrix $\mathbf{\Sigma}$ as well as the pilot matrix \mathbf{S}^T determines the computational complexity of $\hat{\mathbf{h}}_{\text{MMSE}}$ through $\mathbf{\Omega}_b$ that is embedded in \mathbf{C} (see (28)). The number of transmit antennas N_T is not involved in computing the orthant probabilities.

Since the Gaussian orthant probability plays a central role in the expressions for $\hat{\mathbf{h}}_{\text{MMSE}}$ in (40)–(41), we will study the orthant probability more deeply in the next section.

IV. ORTHANT PROBABILITY OF A REAL-VALUED MVN DISTRIBUTION

Referring back to (36), we define

$$\boldsymbol{\Psi}_{\text{std}} = \left[\widetilde{\text{diag}}(\boldsymbol{\Psi}) \right]^{-\frac{1}{2}} \boldsymbol{\Psi} \left[\widetilde{\text{diag}}(\boldsymbol{\Psi}) \right]^{-\frac{1}{2}}. \quad (42)$$

Here, $\boldsymbol{\Psi}_{\text{std}}$ denotes the covariance matrix of the standardized version of L zero-mean random variables whose original covariance matrix is $\boldsymbol{\Psi}$ in (36) [35]. The diagonal elements of $\boldsymbol{\Psi}_{\text{std}}$ are all equal to one, while the off-diagonal elements represent the correlation coefficients between the random variables defined by $\boldsymbol{\Psi}$. Let

$$[\boldsymbol{\Psi}_{\text{std}}]_{ik} = \psi_{ik} \in (-1, 1) \quad (i \neq k, i, k = 1, \dots, L). \quad (43)$$

Through a change of variables, one can readily show that [27]

$$\mathcal{P}(\boldsymbol{\Psi}_{\text{std}}) = \mathcal{P}(\boldsymbol{\Psi}). \quad (44)$$

In [26], [27], [30], it was shown that, for $L = 2$,

$$\mathcal{P}(\boldsymbol{\Psi}) = \frac{1}{4} + \frac{\arcsin(\psi_{12})}{2\pi}, \quad (45)$$

and, for $L = 3$,

$$\mathcal{P}(\boldsymbol{\Psi}) = \frac{1}{8} + \frac{\sum_{i=1}^2 \sum_{k=i+1}^3 \arcsin(\psi_{ik})}{4\pi}. \quad (46)$$

Furthermore, for $L = 4$, an explicit expression for $\mathcal{P}(\boldsymbol{\Psi})$ is provided in Appendix A based on [27], which requires finite integration with one variable. There is no general closed-form expression for $\mathcal{P}(\boldsymbol{\Psi})$ when $L \geq 4$ [27]–[29]. In [27, Eq. (6)], an expression for the orthant probability was derived based on characteristic functions, where the number of terms to be

evaluated grows exponentially with L and the complexity of evaluating some individual integral terms also grows with L . Alternatively, one can use Monte Carlo methods to compute (36), e.g., the algorithm in [31] that was used in [19]. However, Monte Carlo methods also incur a high computational load when L becomes large, which, in turn, generally implies a high computational complexity for determining $\hat{\mathbf{h}}_{\text{MMSE}}$ with large values of N_R and/or τ .

Lemma 1. *Let $\mathbf{q} = [q_1 \ q_2]^T$, with $q_1, q_2 \in \{\pm 1\}$. Let $p(\mathbf{u})$, the pdf of the real-valued random vector $\mathbf{u} = [u_1 \ u_2]^T$, be given by $\mathcal{N}(\mathbf{0}, \Phi)$, with $[\Phi]_{ii} = \sigma_{u_i}^2$, $i = 1, 2$, and $[\Phi]_{12} = [\Phi]_{21} = q_1 q_2 \phi_{12} \sigma_{u_1} \sigma_{u_2}$, $\phi_{12} \in (-1, 1)$. Let $\Lambda_{\mathbf{q}} = \text{diag}(\mathbf{q})$. Then, the vector*

$$\Lambda_{\mathbf{q}} \int_{\mathbb{R}_+^2} \mathbf{u} p(\mathbf{u}) d\mathbf{u} \Big/ \int_{\mathbb{R}_+^2} p(\mathbf{u}) d\mathbf{u} \quad (47)$$

is linear in \mathbf{q} .

Proof: Based on (44) and (45),

$$\int_{\mathbb{R}_+^2} p(\mathbf{u}) d\mathbf{u} = \mathcal{P}(\Phi) = \frac{1}{4} + \frac{q_1 q_2 \arcsin(\phi_{12})}{2\pi}. \quad (48)$$

Based on the reduction in (32)–(34), we obtain

$$\int_{\mathbb{R}_+^2} \mathbf{u} p(\mathbf{u}) d\mathbf{u} = \frac{1 + q_1 q_2 \phi_{12}}{2\sqrt{2}\pi} [\sigma_{u_1} \ \sigma_{u_2}]^T. \quad (49)$$

Inserting (48)–(49) into (47) and capitalizing on the fact that $q_1, q_2 \in \{\pm 1\}$, after some algebraic manipulations we obtain

$$\begin{aligned} & \Lambda_{\mathbf{q}} \int_{\mathbb{R}_+^2} \mathbf{u} p(\mathbf{u}) d\mathbf{u} \Big/ \int_{\mathbb{R}_+^2} p(\mathbf{u}) d\mathbf{u} \\ &= \frac{\begin{bmatrix} \sigma_{u_1} \left(1 - \frac{\phi_{12} \arcsin(\phi_{12})}{\pi/2}\right) & \sigma_{u_1} \left(\phi_{12} - \frac{\arcsin(\phi_{12})}{\pi/2}\right) \\ \sigma_{u_2} \left(\phi_{12} - \frac{\arcsin(\phi_{12})}{\pi/2}\right) & \sigma_{u_2} \left(1 - \frac{\phi_{12} \arcsin(\phi_{12})}{\pi/2}\right) \end{bmatrix} \mathbf{q}}{\sqrt{\frac{\pi}{2}} \left(1 - \left(\frac{\arcsin(\phi_{12})}{\pi/2}\right)^2\right)}. \end{aligned} \quad (50)$$

Remark 4. Relation between Lemma 1 and the optimality of the BLMMSE estimator: Lemma 1 holds based on the use of one-bit symmetric quantization, i.e., $q_1, q_2 \in \{\pm 1\}$. This linearity does not hold generally when \mathbf{u} and \mathbf{q} have three or more elements, as shown in Appendix B. These results are pivotal in determining the condition for the BLMMSE estimator to be MSE-optimal, which will be presented in the next section.

V. CONDITION FOR THE OPTIMALITY OF THE BLMMSE ESTIMATOR

The equivalence between the BLMMSE and MMSE channel estimators for one-bit quantized SISO systems with a single pilot symbol or one-bit quantized noiseless SISO systems with multiple specifically chosen pilots was shown in [19]. Here, our objective is to establish a general condition for their equivalence in one-bit quantized MIMO systems.

Defining

$$\mathbf{D}_{\Omega} = \widehat{\text{diag}}(\Omega_b) \quad (51)$$

from (21), the BLMMSE channel estimate for the system setup in Section II-A can be expressed as [7]

$$\begin{aligned} \hat{\mathbf{h}}_{\text{BLM}} &= \frac{\sqrt{\pi}}{2} \Sigma \mathbf{A}^H \mathbf{D}_{\Omega}^{-\frac{1}{2}} \left(\arcsin \left(\mathbf{D}_{\Omega}^{-\frac{1}{2}} \Re(\Omega_b) \mathbf{D}_{\Omega}^{-\frac{1}{2}} \right) \right. \\ &\quad \left. + j \arcsin \left(\mathbf{D}_{\Omega}^{-\frac{1}{2}} \Im(\Omega_b) \mathbf{D}_{\Omega}^{-\frac{1}{2}} \right) \right)^{-1} \mathbf{r}. \end{aligned} \quad (52)$$

Theorem 1. Necessary and sufficient condition for the BLMMSE channel estimator to be MSE-optimal: Assuming Rayleigh flat fading, spatially and temporally white Gaussian noise, and one-bit ADCs, the BLMMSE channel estimator is MSE-optimal if and only if the off-diagonal elements of \mathbf{C} in (28) satisfy $[\mathbf{C}]_{il} \neq 0$ for at most one value of l other than $l = i$, i.e., an element z_i of the random vector \mathbf{z} defined in (29) is correlated with at most one other element z_l , for $l, i = 1, \dots, 2\tau N_R$ and $l \neq i$.

Proof: First, we show that when the condition on \mathbf{C} in (28) is satisfied, the BLMMSE channel estimator is optimal. Note that $\frac{1}{2}\mathbf{C}^{-1}$ represents the covariance matrix of \mathbf{z} in (29). Based on (28), a suitable permutation matrix Γ is introduced to make $\Gamma \mathbf{C} \Gamma^T = \mathbf{C}_{\text{perm}}$ block-diagonal with 2×2 blocks, with $\Gamma \Gamma^T = \Gamma^T \Gamma = \mathbf{I}_{2\tau N_R}$. These 2×2 sub-matrices can be diagonal. Let $\mathbf{M} = \frac{1}{2}\mathbf{C}_{\text{perm}}^{-1}$ and note that \mathbf{M} is also block-diagonal with 2×2 blocks. For $i = 1, \dots, \tau N_R$, the i -th diagonal block of \mathbf{M} , denoted as \mathbf{M}_i , represents the cross-covariance between a pair of correlated random variables if its off-diagonal elements are non-zero. Furthermore, $\mathcal{P}(\mathbf{M}) = \prod_{i=1}^{\tau N_R} \mathcal{P}(\mathbf{M}_i)$. The pdf of $\mathbf{t} = \Gamma \mathbf{z}$, denoted by $p(\mathbf{t})$, is given by $\mathcal{N}(\mathbf{0}, \mathbf{M})$. After applying this change of variable to (31), we obtain

$$\begin{aligned} \hat{\mathbf{h}}_{\text{BLMMSE}} &= \Sigma \mathbf{A}^H \Omega_b^{-1} [\Lambda_R \ j \Lambda_I] \Gamma^T \\ &\quad \cdot \frac{\int_{\mathbb{R}_+^{2\tau N_R}} \frac{\mathbf{t} \exp\left\{-\frac{\mathbf{t}^T \mathbf{M}^{-1} \mathbf{t}}{2}\right\}}{(2\pi)^{\tau N_R} |\mathbf{M}|^{\frac{1}{2}}} d\mathbf{t}}{\int_{\mathbb{R}_+^{2\tau N_R}} \frac{\exp\left\{-\frac{\mathbf{t}^T \mathbf{M}^{-1} \mathbf{t}}{2}\right\}}{(2\pi)^{\tau N_R} |\mathbf{M}|^{\frac{1}{2}}} d\mathbf{t}} \\ &= \Sigma \mathbf{A}^H \Omega_b^{-1} [\mathbf{I}_{\tau N_R} \ \mathbf{I}_{\tau N_R}] \Gamma^T \\ &\quad \cdot \Gamma \text{diag}([\mathbf{r}_R^T \ j \mathbf{r}_I^T]^T) \Gamma^T \frac{\int_{\mathbb{R}_+^{2\tau N_R}} \mathbf{t} p(\mathbf{t}) d\mathbf{t}}{\mathcal{P}(\mathbf{M})}. \end{aligned} \quad (53)$$

The vector \mathbf{t} defined above can be written as the concatenation of τN_R 2-dimensional vectors, i.e.,

$$\mathbf{t} = [\tilde{\mathbf{t}}_i]_{i=1}^{\tau N_R} = [\tilde{\mathbf{t}}_1^T \ \dots \ \tilde{\mathbf{t}}_{\tau N_R}^T]^T, \quad (55)$$

where $\tilde{\mathbf{t}}_i$ consists of t_{2i-1} and t_{2i} from \mathbf{t} , $i = 1, \dots, \tau N_R$. Using the notation in (55), we have

$$\frac{\int_{\mathbb{R}_+^{2\tau N_R}} \mathbf{t} p(\mathbf{t}) d\mathbf{t}}{\mathcal{P}(\mathbf{M})} = \left[\frac{\left(\int_{\mathbb{R}_+^2} \tilde{\mathbf{t}}_k p(\tilde{\mathbf{t}}_k) d\tilde{\mathbf{t}}_k \right) \prod_{\substack{i=1 \\ i \neq k}}^{\tau N_R} \mathcal{P}(\mathbf{M}_i)}{\mathcal{P}(\mathbf{M})} \right]_{k=1}^{\tau N_R} \quad (56)$$

$$= \left[\frac{\int_{\mathbb{R}_+^2} \tilde{\mathbf{t}}_1^T p(\tilde{\mathbf{t}}_1) d\tilde{\mathbf{t}}_1}{\mathcal{P}(\mathbf{M}_1)} \cdots \frac{\int_{\mathbb{R}_+^{2\tau N_R}} \tilde{\mathbf{t}}_{\tau N_R}^T p(\tilde{\mathbf{t}}_{\tau N_R}) d\tilde{\mathbf{t}}_{\tau N_R}}{\mathcal{P}(\mathbf{M}_{\tau N_R})} \right]^T. \quad (57)$$

Since each component of (57) is the ratio of two integrals as in (47), we conclude based on Lemma 1 and (50) that

$$\mathbf{\Gamma} \text{diag}([\mathbf{r}_R^T \ j\mathbf{r}_I^T]^T) \mathbf{\Gamma}^T \int_{\mathbb{R}_+^{2\tau N_R}} \frac{\mathbf{t}p(\mathbf{t})}{\mathcal{P}(\mathbf{M})} d\mathbf{t} \quad (58)$$

is linear in \mathbf{r}_R and \mathbf{r}_I . Therefore, $\hat{\mathbf{h}}_{\text{MMSE}}$ in (54) is linear in \mathbf{r} . Since the BLMMSE estimator has the smallest MSE [7], [24] among all linear estimators, the BLMMSE estimator must be MSE-optimal.

Conversely, when the BLMMSE estimator is optimal, i.e., when $\hat{\mathbf{h}}_{\text{MMSE}}$ is linear in \mathbf{r} , based on Remark 4 and Appendix B, there cannot be any full $m \times m$ (with $m \geq 3$) sub-matrix in $\frac{1}{2}\mathbf{C}^{-1}$ with only non-zero elements. The dimension of any full sub-matrix of $\frac{1}{2}\mathbf{C}^{-1}$ must be at most 2×2 . The same can be concluded for \mathbf{C} . ■

The proof of Theorem 1 hinges on Lemma 1 as well as Remark 4 and Appendix B. Guided by this framework, below we present specific cases where $\hat{\mathbf{h}}_{\text{MMSE}}$ is directly computed to be equivalent to $\hat{\mathbf{h}}_{\text{BLM}}$.

A. Spatially White Channel and Unitary Pilot Matrix

Here, we assume $\mathbf{\Sigma} = \mathbf{I}_{N_T N_R}$ and a unitary pilot matrix with $\tau = N_T$. Thus, $\mathbf{S}\mathbf{S}^H = \eta\mathbf{I}$, with $\eta > 0$, and

$$\mathbf{D}_R = \frac{1}{\eta + \sigma^2} \mathbf{I}_{\tau N_R}, \quad \mathbf{D}_I = \mathbf{0}. \quad (59)$$

For this case, $\mathbf{C} = \text{DIAG}(\mathbf{D}_R, \mathbf{D}_R)$ is diagonal, thereby satisfying the condition of Theorem 1.

Due to the fact that $\mathbf{D}_I = \mathbf{0}$, from (29) and (31) we have

$$\hat{\mathbf{h}}_{\text{MMSE}} = \mathbf{\Sigma} \mathbf{A}^H \mathbf{\Omega}_b^{-1} \left(\frac{\mathbf{\Lambda}_R \int_{\mathbb{R}_+^{\tau N_R}} \mathbf{x} e^{-\mathbf{x}^T \mathbf{\Lambda}_R \mathbf{D}_R \mathbf{\Lambda}_R \mathbf{x}} d\mathbf{x}}{\int_{\mathbb{R}_+^{\tau N_R}} e^{-\mathbf{x}^T \mathbf{\Lambda}_R \mathbf{D}_R \mathbf{\Lambda}_R \mathbf{x}} d\mathbf{x}} + \frac{j\mathbf{\Lambda}_I \int_{\mathbb{R}_+^{\tau N_R}} \mathbf{y} e^{-\mathbf{y}^T \mathbf{\Lambda}_I \mathbf{D}_R \mathbf{\Lambda}_I \mathbf{y}} d\mathbf{y}}{\int_{\mathbb{R}_+^{\tau N_R}} e^{-\mathbf{y}^T \mathbf{\Lambda}_I \mathbf{D}_R \mathbf{\Lambda}_I \mathbf{y}} d\mathbf{y}} \right). \quad (60)$$

Further calculations based on (59)–(60) and (52) lead to

$$\hat{\mathbf{h}}_{\text{MMSE}} = \frac{(\mathbf{S}^H \otimes \mathbf{I}_{N_R}) \mathbf{r}}{\sqrt{\pi(\eta + \sigma^2)}} = \hat{\mathbf{h}}_{\text{BLM}}. \quad (61)$$

Remark 5. Based on (61), for a spatially white Rayleigh fading channel with a unitary pilot matrix, the low-complexity BLMMSE estimator is MSE-optimal and thus its use is justified for low spatial correlation. A similar conclusion was reached in [19], but only for the SIMO case with a single pilot symbol.

The above result can be generalized even further, as shown next.

B. Transmit-Only Channel Correlation

Assume $\tau = N_T$ and let $\mathbf{H} = \mathbf{H}_w \mathbf{\Sigma}_{\text{TX}}^{\frac{1}{2}}$, where the elements of \mathbf{H}_w are i.i.d. $\mathcal{CN}(0, 1)$ random variables. Then, $\mathbf{h} = \text{vec}(\mathbf{H}) \sim \mathcal{CN}(\mathbf{0}, \mathbf{\Sigma})$, with $\mathbf{\Sigma} = \mathbf{\Sigma}_{\text{TX}} \otimes \mathbf{I}_{N_R}$. Denote the eigenvalue decomposition of $\mathbf{\Sigma}_{\text{TX}}$ as

$$\mathbf{\Sigma}_{\text{TX}} = \mathbf{U} \mathbf{\Xi} \mathbf{U}^H, \quad \mathbf{\Xi} = \text{diag}([\xi_i]_{i=1}^{N_T}), \quad (62)$$

with $\xi_i > 0$, $\forall i$. Setting $\mathbf{S} = \sqrt{\eta} \mathbf{U}^H$, it can be shown that $\mathbf{D}_R = \text{diag}\left(\left[\frac{1}{\eta\xi_i + \sigma^2}\right]_{i=1}^{N_T}\right) \otimes \mathbf{I}_{N_R}$ and $\mathbf{D}_I = \mathbf{0}$. Moreover, $\mathbf{C} = \text{DIAG}(\mathbf{D}_R, \mathbf{D}_R)$ is diagonal and satisfies the condition in Theorem 1. Since $\mathbf{D}_I = \mathbf{0}$, (60) holds again and the integrals therein are over scalar variables. Finally, it is straightforward to show that

$$\hat{\mathbf{h}}_{\text{MMSE}} = \left(\left(\mathbf{U} \text{diag} \left(\left[\frac{\xi_i \sqrt{\eta}}{\sqrt{\eta\xi_i + \sigma^2}} \right]_{i=1}^{N_T} \right) \right) \otimes \mathbf{I}_{N_R} \right) \frac{\mathbf{r}}{\sqrt{\pi}} \quad (63)$$

$$= \hat{\mathbf{h}}_{\text{BLM}}. \quad (64)$$

Clearly, (61) is a special case of (64) with $\mathbf{\Sigma}_{\text{TX}} = \mathbf{I}_{N_T}$. If $\mathbf{\Sigma}_{\text{TX}}$ is circulant, then a Fourier matrix can be used as pilot matrix.

Remark 6. Assume a standardized $\mathbf{\Sigma}_{\text{TX}}$ as in (42). Based on (64) and [7], [17], it can be shown that, when the pilot symbol power is sufficiently high or, equivalently, when the noise power is sufficiently low, the MSE per antenna for both estimators is given by $1 - \frac{2}{\pi}$, i.e.,

$$\lim_{\sigma^2 \rightarrow 0} \frac{\mathbb{E}(\|\hat{\mathbf{h}}_{\text{MMSE}} - \mathbf{h}\|^2)}{N_T N_R} = \lim_{\sigma^2 \rightarrow 0} \frac{\mathbb{E}(\|\hat{\mathbf{h}}_{\text{BLM}} - \mathbf{h}\|^2)}{N_T N_R} \quad (65)$$

$$= 1 - \frac{2}{\pi}. \quad (66)$$

C. Spatially White Channel with $\tau = 2$ Real-Valued Pilots

Here, $\mathbf{\Sigma} = \mathbf{I}_{N_T N_R}$ and $\tau = 2$. Let $\mathbf{s}_1, \mathbf{s}_2$ be two real-valued N_T -dimensional pilot vectors in (1) and $\mathbf{S}^T = [\mathbf{s}_1 \ \mathbf{s}_2]$. Clearly, $\mathbf{D}_R = (\mathbf{S}\mathbf{S}^T + \sigma^2 \mathbf{I}_2)^{-1} \otimes \mathbf{I}_{N_R}$. Moreover, $\mathbf{D}_I = \mathbf{0}$ and (60) holds. Defining

$$\mathbf{\Delta}_R = \text{diag}\left([r_{R,i} r_{R,N_R+i}]_{i=1}^{N_R}\right), \quad (67)$$

$$\mathbf{\Delta}_I = \text{diag}\left([r_{I,i} r_{I,N_R+i}]_{i=1}^{N_R}\right), \quad (68)$$

$$\mathbf{C}_{\text{sub},R} = \begin{bmatrix} (\|\mathbf{s}_2\|^2 + \sigma^2) \mathbf{I}_{N_R} & -\mathbf{s}_1^T \mathbf{s}_2 \mathbf{\Delta}_R \\ -\mathbf{s}_1^T \mathbf{s}_2 \mathbf{\Delta}_R & (\|\mathbf{s}_1\|^2 + \sigma^2) \mathbf{I}_{N_R} \end{bmatrix}, \quad (69)$$

and letting $\mathbf{C}_{\text{sub},I}$ be identical to $\mathbf{C}_{\text{sub},R}$ except that all $\mathbf{\Delta}_R$ terms are replaced by $\mathbf{\Delta}_I$, we obtain

$$\mathbf{C} = \frac{\text{DIAG}(\mathbf{C}_{\text{sub},R}, \mathbf{C}_{\text{sub},I})}{|\mathbf{S}\mathbf{S}^T + \sigma^2 \mathbf{I}_2|}. \quad (70)$$

Since x_i and x_{i+N_R} , as well as y_i and y_{i+N_R} , $i = 1, \dots, N_R$, are pair-wise correlated, Theorem 1 holds. Define

$$\mathbf{s}_{1,\text{new}} = \frac{\mathbf{s}_1}{\sqrt{\|\mathbf{s}_1\|^2 + \sigma^2}}, \quad \mathbf{s}_{2,\text{new}} = \frac{\mathbf{s}_2}{\sqrt{\|\mathbf{s}_2\|^2 + \sigma^2}}, \quad (71)$$

$\gamma_s = \mathbf{s}_{1,\text{new}}^T \mathbf{s}_{2,\text{new}}$, and $\mathbf{S}_{w1}^T = [\mathbf{s}_{1,\text{new}} \ \mathbf{s}_{2,\text{new}}]$. Using the method in the proof of Theorem 1, we obtain

$$\hat{\mathbf{h}}_{\text{MMSE}} = \hat{\mathbf{h}}_{\text{BLM}} \quad (72)$$

$$= \left(\left(\mathbf{S}_{w1}^T \begin{bmatrix} 1 & \frac{\arcsin(\gamma_s)}{\pi/2} \\ \frac{\arcsin(\gamma_s)}{\pi/2} & 1 \end{bmatrix}^{-1} \right) \otimes \mathbf{I}_{N_R} \right) \frac{\mathbf{r}}{\sqrt{\pi}}. \quad (73)$$

D. Spatially White Channel and $\tau = 2$ Complex-Valued Pilots with $\pi/2$ Phase Difference

Let $\tau = 2$ and $\Sigma = \mathbf{I}_{N_T N_R}$. By assumption,

$$\mathbf{S}^T = [\mathbf{s}_1 \ \mathbf{s}_2], \quad \frac{\mathbf{s}_2}{\|\mathbf{s}_2\|} = j \frac{\mathbf{s}_1}{\|\mathbf{s}_1\|}. \quad (74)$$

Then,

$$\mathbf{S}\mathbf{S}^H = \begin{bmatrix} \|\mathbf{s}_1\|^2 & -j\|\mathbf{s}_1\|\|\mathbf{s}_2\| \\ j\|\mathbf{s}_1\|\|\mathbf{s}_2\| & \|\mathbf{s}_2\|^2 \end{bmatrix}, \quad (75)$$

$$\mathbf{D}_R = \frac{\text{diag}([\|\mathbf{s}_2\|^2 + \sigma^2 \ \|\mathbf{s}_1\|^2 + \sigma^2]^T) \otimes \mathbf{I}_{N_R}}{\sigma^2 [\sigma^2 + \text{tr}(\mathbf{S}\mathbf{S}^H)]}, \quad (76)$$

$$\mathbf{D}_I = \frac{\begin{bmatrix} 0 & \|\mathbf{s}_1\|\|\mathbf{s}_2\| \\ -\|\mathbf{s}_1\|\|\mathbf{s}_2\| & 0 \end{bmatrix} \otimes \mathbf{I}_{N_R}}{\sigma^2 (\sigma^2 + \text{tr}(\mathbf{S}\mathbf{S}^H))}. \quad (77)$$

Here, (60) no longer holds. However, by defining

$$\Delta_X = \text{diag}([r_{R,i} r_{1,N_R+i}]_{i=1}^{N_R}), \quad (78)$$

$$\Delta_Y = \text{diag}([r_{1,i} r_{R,N_R+i}]_{i=1}^{N_R}), \quad (79)$$

$$\mathbf{C}_{\text{sub,A}} = \text{DIAG}([\|\mathbf{s}_2\|^2 + \sigma^2 \ \|\mathbf{s}_1\|^2 + \sigma^2] \mathbf{I}_{N_R}), \quad (80)$$

$$\mathbf{C}_{\text{sub,B}} = \begin{bmatrix} \mathbf{0} & -\|\mathbf{s}_1\|\|\mathbf{s}_2\| \Delta_X \\ \|\mathbf{s}_1\|\|\mathbf{s}_2\| \Delta_Y & \mathbf{0} \end{bmatrix}, \quad (81)$$

we have

$$\mathbf{C} = \frac{1}{\sigma^2 (\sigma^2 + \text{tr}(\mathbf{S}\mathbf{S}^H))} \begin{bmatrix} \mathbf{C}_{\text{sub,A}} & \mathbf{C}_{\text{sub,B}} \\ \mathbf{C}_{\text{sub,B}}^T & \mathbf{C}_{\text{sub,A}} \end{bmatrix}, \quad (82)$$

which clearly satisfies the condition in Theorem 1. Reusing the definitions from (71) in the new context here, denote $\tilde{\gamma}_s = \|\mathbf{s}_{1,\text{new}}\| \|\mathbf{s}_{2,\text{new}}\|$ and $\mathbf{S}_{w2}^H = [\mathbf{s}_{1,\text{new}}^* \ \mathbf{s}_{2,\text{new}}^*]$. Then, (31) yields

$$\hat{\mathbf{h}}_{\text{MMSE}} = \hat{\mathbf{h}}_{\text{BLM}} \quad (83)$$

$$= \left(\left(\mathbf{S}_{w2}^H \begin{bmatrix} 1 & \frac{-j \arcsin(\tilde{\gamma}_s)}{\pi/2} \\ \frac{j \arcsin(\tilde{\gamma}_s)}{\pi/2} & 1 \end{bmatrix}^{-1} \right) \otimes \mathbf{I}_{N_R} \right) \frac{\mathbf{r}}{\sqrt{\pi}}. \quad (84)$$

Corollary 1. *With $N_T = 1$, $\tau = 2$, and arbitrary N_R , $\hat{\mathbf{h}}_{\text{BLM}}$ and $\hat{\mathbf{h}}_{\text{MMSE}}$ are equivalent for spatially white channels if QPSK symbols are used as pilot symbols.*

Proof: If the phase difference of the two pilot symbol s_1 and s_2 is π , the result in Section V-C applies. If the phase difference is $\frac{\pi}{2}$, the result in Section V-D applies. In both cases, the condition in Theorem 1 is satisfied. ■

E. SIMO with Real-Valued Channel Correlation, $N_R = 2$, and $\tau = N_T = 1$

The non-linearity of the MMSE channel estimate for noiseless correlated SIMO channels was considered in [19]. Here, we focus on a general noisy correlated SIMO channel with a single complex-valued pilot symbol (i.e., $\tau = N_T = 1$) and the system model (2) becomes

$$\mathbf{y} = \mathbf{s}\mathbf{h} + \mathbf{n}. \quad (85)$$

Let Σ be real-valued, e.g., as in the exponential channel model [36], [37]. Then,

$$\mathbf{D}_R^{-1} = \Omega_b = |s|^2 \Sigma + \sigma^2 \mathbf{I}_{N_R}, \quad \mathbf{D}_I = \mathbf{0}, \quad (86)$$

and (60) holds. Furthermore, $\mathbf{C} = \frac{1}{2} \text{DIAG}(\mathbf{W}_R^{-1}, \mathbf{W}_I^{-1})$, with

$$\mathbf{W}_R = \frac{1}{2} \Lambda_R \mathbf{D}_R^{-1} \Lambda_R, \quad \mathbf{W}_I = \frac{1}{2} \Lambda_I \mathbf{D}_R^{-1} \Lambda_I. \quad (87)$$

Hence, (60) is equivalent to

$$\hat{\mathbf{h}}_{\text{MMSE}} = s^* \Sigma \mathbf{D}_R \left(\frac{\Lambda_R \int_{\mathbb{R}_+^{N_R}} \mathbf{x} e^{-\frac{\mathbf{x}^T \mathbf{W}_R^{-1} \mathbf{x}}{2}} d\mathbf{x}}{\int_{\mathbb{R}_+^{N_R}} e^{-\frac{\mathbf{x}^T \mathbf{W}_R^{-1} \mathbf{x}}{2}} d\mathbf{x}} + \frac{j \Lambda_I \int_{\mathbb{R}_+^{N_R}} \mathbf{y} e^{-\frac{\mathbf{y}^T \mathbf{W}_I^{-1} \mathbf{y}}{2}} d\mathbf{y}}{\int_{\mathbb{R}_+^{N_R}} e^{-\frac{\mathbf{y}^T \mathbf{W}_I^{-1} \mathbf{y}}{2}} d\mathbf{y}} \right). \quad (88)$$

When $N_R = 2$, given the structure of \mathbf{C} above, Theorem 1 holds trivially. Consistent with this observation, based on Lemma 1, the two ratios in (88) are linear in \mathbf{r}_R and \mathbf{r}_I , respectively. Assume a standardized Σ and denote the correlation coefficient as ρ_{12} . Defining $\beta_{12} = \frac{\rho_{12}|s|^2}{|s|^2 + \sigma^2}$, we obtain

$$\hat{\mathbf{h}}_{\text{MMSE}} = \frac{s^* \Sigma \begin{bmatrix} 1 & \frac{\arcsin(\beta_{12})}{\pi/2} \\ \frac{\arcsin(\beta_{12})}{\pi/2} & 1 \end{bmatrix}^{-1} \mathbf{r}}{\sqrt{\pi}(|s|^2 + \sigma^2)} = \hat{\mathbf{h}}_{\text{BLM}}. \quad (89)$$

VI. CASES WITH NONLINEAR MMSE ESTIMATORS

We now consider two cases where the assumption of Theorem 1 does not hold and thus $\hat{\mathbf{h}}_{\text{MMSE}}$ is non-linear in \mathbf{r} . For general MIMO systems with arbitrary channel correlation and pilots, one can always resort to our explicit expressions in (40)–(41) and use existing methods discussed in Section IV (e.g., the algorithm for Monte Carlo simulations in [31]) to compute the required Gaussian orthant probabilities for one covariance matrix of dimension $(2\tau N_R) \times (2\tau N_R)$ and $2\tau N_R$ covariance matrices of dimension $(2\tau N_R - 1) \times (2\tau N_R - 1)$. Clearly, when either τ or N_R is large, Monte Carlo methods become computationally cumbersome and cannot guarantee accuracy. Nevertheless, using our insights above (e.g., Remark 2) and existing results on Gaussian orthant probabilities, computationally efficient analytical expressions for $\hat{\mathbf{h}}_{\text{MMSE}}$ can be derived for various SIMO channels under specific assumptions on the channel correlation or pilot symbols.

A. SIMO with Real-Valued Correlation, $N_R > 2$, and $\tau = N_T = 1$

Consider the same SIMO system described by (85) in Section V-E with $\tau = N_T = 1$ and $N_R > 2$. In this case, (86)–(88) remain applicable. Without loss of generality, let the channel covariance matrix Σ be standardized and let the correlation coefficients be denoted as ρ_{ik} , for $i, k = 1, \dots, N_R$ and $i \neq k$, unless otherwise stated.

Let $\mathbf{D}_{R,-k}$ denote the $(N_R - 1) \times (N_R - 1)$ matrix obtained by deleting the k -th row and column of \mathbf{D}_R . Likewise, let $\Lambda_{R,-k}$ (resp. $\Lambda_{I,-k}$) denote the $(N_R - 1) \times (N_R - 1)$ matrix obtained by deleting the k -th row and column of Λ_R (resp. Λ_I). Moreover, for $k = 1, \dots, N_R$, define

$$\mathbf{W}_{x,k} = \frac{1}{2} \Lambda_{R,-k} \mathbf{D}_{R,-k}^{-1} \Lambda_{R,-k}, \quad (90)$$

$$\mathbf{W}_{y,k} = \frac{1}{2} \Lambda_{I,-k} \mathbf{D}_{R,-k}^{-1} \Lambda_{I,-k}. \quad (91)$$

Using the definitions of \mathbf{W}_R and \mathbf{W}_I in (87), it is shown in Appendix C that

$$\hat{\mathbf{h}}_{\text{MMSE}} = \frac{s^* \Sigma}{2\sqrt{\pi}(|s|^2 + \sigma^2)} \left(\frac{\Lambda_R \mathbf{g}_R}{\mathcal{P}(\mathbf{W}_R)} + \frac{j \Lambda_I \mathbf{g}_I}{\mathcal{P}(\mathbf{W}_I)} \right), \quad (92)$$

where the k -th element of \mathbf{g}_R (resp. \mathbf{g}_I) is equal to $\mathcal{P}(\mathbf{W}_{x,k})$ (resp. $\mathcal{P}(\mathbf{W}_{y,k})$). When $N_R = 2$, (92) reduces to (89) in Section V-E. When $N_R \geq 3$, (92) is the starting point for further results below.

Theorem 2. Consider the one-bit quantized, spatially correlated Rayleigh fading SIMO system given by (85) with $N_T = \tau = 1$ and $N_R = 3$. Then,

$$\hat{\mathbf{h}}_{\text{MMSE}} = \frac{s^* \Sigma}{2\sqrt{\pi}(|s|^2 + \sigma^2)} \left(\frac{\mathbf{v}_{3R}}{P_{3R}} + j \frac{\mathbf{v}_{3I}}{P_{3I}} \right), \quad (93)$$

with

$$\beta_{ik} = \frac{\rho_{ik}|s|^2}{|s|^2 + \sigma^2}, \quad (i \neq k, i, k = 1, 2, 3) \quad (93a)$$

$$\mathbf{v}_{3R} = \begin{bmatrix} \frac{r_{R,1}}{4} + \frac{r_{R,1}r_{R,2}r_{R,3}}{2\pi} \arcsin \left(\frac{\beta_{23} - \beta_{12}\beta_{13}}{\sqrt{1-\beta_{12}^2}\sqrt{1-\beta_{13}^2}} \right) \\ \frac{r_{R,2}}{4} + \frac{r_{R,1}r_{R,2}r_{R,3}}{2\pi} \arcsin \left(\frac{\beta_{13} - \beta_{12}\beta_{23}}{\sqrt{1-\beta_{12}^2}\sqrt{1-\beta_{23}^2}} \right) \\ \frac{r_{R,3}}{4} + \frac{r_{R,1}r_{R,2}r_{R,3}}{2\pi} \arcsin \left(\frac{\beta_{12} - \beta_{13}\beta_{23}}{\sqrt{1-\beta_{13}^2}\sqrt{1-\beta_{23}^2}} \right) \end{bmatrix}, \quad (93b)$$

$$P_{3R} = \frac{1}{8} + \frac{\sum_{i=1}^2 \sum_{k=i+1}^3 r_{R,i} r_{R,k} \arcsin(\beta_{ik})}{4\pi}, \quad (93c)$$

and where \mathbf{v}_{3I} (resp. P_{3I}) is the same as \mathbf{v}_{3R} (resp. P_{3R}) except that $r_{R,i}$ in (93b) (resp. (93c)) is replaced by $r_{I,i}$ for $i = 1, 2, 3$.

Proof: The proof starts from (92) and is based on (44), (45), and (46). The detailed calculations are similar to those in Appendix B, hence omitted for brevity. ■

On the other hand, under the same assumptions for Theorem 2, the BLMMSE channel estimate is given by

$$\hat{\mathbf{h}}_{\text{BLM}} = \frac{s^* \Sigma \begin{bmatrix} 1 & \frac{\arcsin(\beta_{12})}{\pi/2} & \frac{\arcsin(\beta_{13})}{\pi/2} \\ \frac{\arcsin(\beta_{12})}{\pi/2} & 1 & \frac{\arcsin(\beta_{23})}{\pi/2} \\ \frac{\arcsin(\beta_{13})}{\pi/2} & \frac{\arcsin(\beta_{23})}{\pi/2} & 1 \end{bmatrix}^{-1} \mathbf{r}}{\sqrt{\pi}(|s|^2 + \sigma^2)}. \quad (94)$$

In general, (94) is not equivalent to (93). However, we have $\hat{\mathbf{h}}_{\text{BLM}} = \hat{\mathbf{h}}_{\text{MMSE}}$ if one of the following holds: $\rho_{23} = \rho_{13} = 0$, $\rho_{13} = \rho_{12} = 0$, or $\rho_{12} = \rho_{23} = 0$. This is consistent with Theorem 1.

Remark 7. Theorem 2 is significant that, for one-bit ADCs, it provides the simplest closed-form expression for $\hat{\mathbf{h}}_{\text{MMSE}}$ that demonstrates non-linear dependence on \mathbf{r} .

When $N_R = 4$, for the same SIMO system given by (85) with a real-valued channel covariance matrix, $\mathcal{P}(\mathbf{W}_R)$ and $\mathcal{P}(\mathbf{W}_I)$ in (92) can be obtained based on (109) in Appendix A. In addition, for the 3×3 matrices $\mathbf{W}_{x,k}$ and $\mathbf{W}_{y,k}$, $\mathcal{P}(\mathbf{W}_{x,k})$ and $\mathcal{P}(\mathbf{W}_{y,k})$ required in (92) are calculated using (46), $k = 1, \dots, 4$. Indeed, one can obtain a semi-closed-form expression for (92) with only one-dimensional finite integration from (109). Details are omitted for brevity.

Next, we consider the SIMO system in (85) with arbitrary N_R but with equal positive channel cross-correlation for all pairs of receive antennas. Let $Q(\cdot)$ denote the Q -function, i.e., the right tail distribution function of the standard normal distribution $\mathcal{N}(0, 1)$.

Theorem 3. Consider the one-bit quantized, spatially correlated Rayleigh fading SIMO system given by (85) with $N_T = \tau = 1$. Let the correlation coefficients in Σ be given by $\rho_{ik} = \rho$ (with $0 \leq \rho \leq 1$), for $i, k = 1, \dots, N_R$ and $i \neq k$. Then,

$$\hat{\mathbf{h}}_{\text{MMSE}} = \frac{s^* \Sigma}{2\sqrt{\pi}(|s|^2 + \sigma^2)} \left(\frac{\Lambda_R \mathbf{v}_{RE}}{P_{RE}} + \frac{j \Lambda_I \mathbf{v}_{IM}}{P_{IM}} \right), \quad (95)$$

with

$$P_{RE} = \int_{-\infty}^{\infty} \prod_{k=1}^{N_R} Q \left(\frac{r_{R,k} \sqrt{\rho} |s| t}{\sqrt{|s|^2(1-\rho) + \sigma^2}} \right) \frac{e^{-t^2/2}}{\sqrt{2\pi}} dt, \quad (96)$$

and where P_{IM} is the same as P_{RE} except that $r_{R,k}$ in (96) is replaced by $r_{I,k}$, for $k = 1, \dots, N_R$. The k -th element of \mathbf{v}_{RE} is given by

$$v_{RE,k} = \int_{-\infty}^{\infty} \prod_{i=1, i \neq k}^{N_R} Q \left(\frac{r_{R,i} \sqrt{\rho} |s| t}{\sqrt{|s|^2 + \sigma^2}} \right) \frac{e^{-t^2/2}}{\sqrt{2\pi}} dt, \quad (97)$$

for $k = 1, \dots, N_R$. The k -th element of \mathbf{v}_{IM} , i.e., $v_{IM,k}$, is the same as $v_{RE,k}$ except that $r_{R,i}$ is replaced by $r_{I,i}$ for i in (97) and $k = 1, \dots, N_R$.

Proof: The proof utilizes the key observation made in Remark 2 that each off-diagonal element of \mathbf{C} in (28) is affected by exactly two different elements from $[\mathbf{r}_R^T \ \mathbf{r}_I^T]^T$. In particular, the off-diagonal elements of \mathbf{W}_R and \mathbf{W}_I in (87), as well as those of $\mathbf{W}_{x,k}$ and $\mathbf{W}_{y,k}$ in (90)–(91), for

$k = 1, \dots, N_R$, are each affected by one pair of elements in \mathbf{r}_R and \mathbf{r}_I , respectively. Based on this key fact, the proof further invokes the results in [30, p. 192]. A detailed proof is provided in Appendix D. ■

Remark 8. Both (96) and (97) require integration with only one variable. Therefore, (95) can be conveniently evaluated using common computing software even for large N_R [30].

B. SISO and Spatially White SIMO with Real-Valued Pilots, Arbitrary τ , and $N_T = 1$

For spatially white SIMO systems, the MMSE channel estimate derived for one receive antenna holds for all receive antennas. This allows us to focus on SISO channels with multiple real-valued pilot symbols. Denote the real-valued pilot vector \mathbf{s} as

$$\mathbf{s} = [s_1 \dots s_\tau]^T. \quad (98)$$

When $\tau = 1$, this scenario becomes a special case of Section V-A with $\tau = N_T = N_R = 1$. Furthermore, when $\tau = 2$, the setup reduces to that in Section V-C with $N_T = N_R = 1$. Therefore, the non-trivial new case here corresponds to $\tau > 2$, although subsequent results are applicable to $\tau = 1, 2$.

When $N_R = N_T = 1$, the system model (2) reduces to $\mathbf{y} = h\mathbf{s} + \mathbf{n}$, with $h \sim \mathcal{CN}(0, 1)$. Correspondingly, we have

$$\mathbf{D}_R = (\mathbf{s}\mathbf{s}^T + \sigma^2\mathbf{I}_\tau)^{-1}, \quad \mathbf{D}_I = \mathbf{0}. \quad (99)$$

Using the Sherman-Morrison formula [34, p. 124], we have $\mathbf{D}_R = \frac{1}{\sigma^2} \left[\mathbf{I}_\tau - \frac{\mathbf{s}\mathbf{s}^T}{\mathbf{s}^T\mathbf{s} + \sigma^2} \right]$. Let $\tilde{\mathbf{D}}_{R,-k}$ denote the $(\tau - 1) \times (\tau - 1)$ matrix obtained by deleting the k -th row and column of \mathbf{D}_R in (99). Then,

$$\tilde{\mathbf{D}}_{R,-k} = \frac{1}{\sigma^2} \left(\mathbf{I}_{\tau-1} - \frac{\mathbf{s}_{-k}\mathbf{s}_{-k}^T}{\mathbf{s}^T\mathbf{s} + \sigma^2} \right), \quad (100)$$

$$\tilde{\mathbf{D}}_{R,-k}^{-1} = \sigma^2 \left(\mathbf{I}_{\tau-1} + \frac{\mathbf{s}_{-k}\mathbf{s}_{-k}^T}{s_k^2 + \sigma^2} \right), \quad (101)$$

where $\mathbf{s}_{-k} = [s_1 \dots s_{k-1} \ s_{k+1} \dots s_\tau]^T$. Define

$$\mathbf{W}_A = \frac{1}{2} \mathbf{\Lambda}_R \mathbf{D}_R^{-1} \mathbf{\Lambda}_R, \quad \mathbf{W}_B = \frac{1}{2} \mathbf{\Lambda}_I \mathbf{D}_R^{-1} \mathbf{\Lambda}_I, \quad (102)$$

and let $\tilde{\mathbf{\Lambda}}_{R,-k}$ (resp. $\tilde{\mathbf{\Lambda}}_{I,-k}$) denote the $(\tau - 1) \times (\tau - 1)$ matrix obtained by deleting the k -th row and column of $\mathbf{\Lambda}_R$ (resp. $\mathbf{\Lambda}_I$). Lastly, define

$$\mathbf{W}_{A,k} = \frac{1}{2} \tilde{\mathbf{\Lambda}}_{R,-k} \tilde{\mathbf{D}}_{R,-k}^{-1} \tilde{\mathbf{\Lambda}}_{R,-k}, \quad (103)$$

$$\mathbf{W}_{B,k} = \frac{1}{2} \tilde{\mathbf{\Lambda}}_{I,-k} \tilde{\mathbf{D}}_{R,-k}^{-1} \tilde{\mathbf{\Lambda}}_{I,-k}. \quad (104)$$

Theorem 4. For a Rayleigh fading SISO channel with a real-valued pilot vector and with one-bit quantization at the receiver, the MMSE channel estimate is given by

$$\hat{h}_{\text{MMSE}} = \frac{1}{2\sqrt{\pi}} \sum_{k=1}^{\tau} s_k \frac{\left(\frac{r_{R,k} \mathcal{P}(\mathbf{W}_{A,k})}{\mathcal{P}(\mathbf{W}_A)} + \frac{j r_{I,k} \mathcal{P}(\mathbf{W}_{B,k})}{\mathcal{P}(\mathbf{W}_B)} \right)}{\sqrt{s_k^2 + \sigma^2}}, \quad (105)$$

with

$$\mathcal{P}(\mathbf{W}_A) = \int_{-\infty}^{\infty} \prod_{i=1}^{\tau} Q \left(\frac{r_{R,i} s_i t}{\sigma} \right) \frac{e^{-\frac{t^2}{2}}}{\sqrt{2\pi}} dt, \quad (106)$$

$$\mathcal{P}(\mathbf{W}_{A,k}) = \int_{-\infty}^{\infty} \prod_{i=1, i \neq k}^{\tau} Q \left(\frac{r_{R,i} s_i t}{\sqrt{s_k^2 + \sigma^2}} \right) \frac{e^{-\frac{t^2}{2}}}{\sqrt{2\pi}} dt, \quad (107)$$

for $k = 1, \dots, \tau$. Note that, $\forall k$, $\mathcal{P}(\mathbf{W}_{B,k})$ is the same as $\mathcal{P}(\mathbf{W}_{A,k})$ in (107) except that $r_{R,i}$ is replaced by $r_{I,i}$, for $i \neq k$. Similarly, $\mathcal{P}(\mathbf{W}_B)$ is the same as $\mathcal{P}(\mathbf{W}_A)$ in (106) except that $r_{R,i}$ is replaced by $r_{I,i}$, $i = 1, \dots, \tau$.

Proof: The main idea is similar to that for the proof of Theorem 3. Details are given in Appendix E. ■

Remark 9. Let $N_T = N_R = 1$. As expected, when $\tau = 1$, (105) is equivalent to (61), whereas when $\tau = 2$, (105) is the same as (73). In both cases, $\hat{h}_{\text{MMSE}} = \hat{h}_{\text{BLM}}$, and the corresponding asymptotic MSE is given by

$$\lim_{\sigma^2 \rightarrow 0} \mathbb{E}(|\hat{h}_{\text{MMSE}} - h|^2) = \lim_{\sigma^2 \rightarrow 0} \mathbb{E}(|\hat{h}_{\text{BLM}} - h|^2) = 1 - \frac{2}{\pi}. \quad (108)$$

In fact, from both (73) and (84), (108) is the asymptotic MSE per antenna for both estimators when the noise power is sufficiently low.

VII. NUMERICAL RESULTS

We now provide simulation results to complement the above analyses. The BLMMSE channel estimate is obtained using (52) from [7] and the corresponding theoretical MSE per antenna can be readily calculated as in [17]. For cases with a single pilot, the signal-to-noise ratio (SNR) is defined as $\text{SNR} = |s|^2/\sigma^2$. For cases with a τ -dimensional pilot vector \mathbf{s} , $\text{SNR} = \|\mathbf{s}\|^2/(\tau\sigma^2)$. When a pilot matrix is used, $\text{SNR} = \text{tr}(\mathbf{S}\mathbf{S}^H)/(\tau N_T \sigma^2)$. The MSE per antenna is averaged over many fading realizations. Without loss of generality, the channel covariance matrices used here are standardized.

A. MISO and MIMO with No Receive Correlation and Unitary Pilot Matrix

Here, we investigate the impact of transmit antenna correlation and the number of transmit antennas N_T for the case considered in Section V-B with $\hat{\mathbf{h}}_{\text{BLM}} = \hat{\mathbf{h}}_{\text{MMSE}}$. In the absence of channel correlation at the receiver for MIMO systems, the MSE is the same for all receive antennas. Therefore, a MISO setup is considered for simplicity. For transmit channel correlation in (62), we use the exponential correlation model [36], [37] and let $[\boldsymbol{\Sigma}_{\text{TX}}]_{ik} = 0.5^{|i-k|}$ or $[\boldsymbol{\Sigma}_{\text{TX}}]_{ik} = 0.9^{|i-k|}$, for $i, k = 1, \dots, N_T$. The results are shown in Fig. 1. Clearly, increasing both N_T and the amount of transmit correlation improves the MSE performance at low SNR. At high SNR, the MSE per antenna converges to $1 - \frac{2}{\pi}$, confirming the claim in Remark 6. Similar trends are observed for other correlation models such as those in [38], [39].

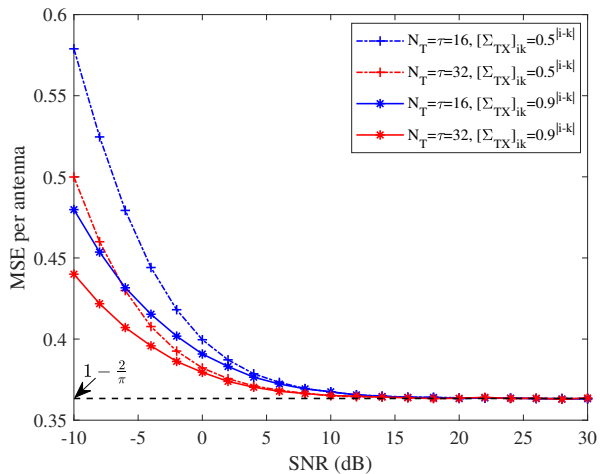


Figure 1. MSE comparison for MISO case with $\tau = N_T = 16, 32$ and exponential transmit correlation model using a tailored pilot matrix. In this scenario $\hat{\mathbf{h}}_{\text{MMSE}} = \hat{\mathbf{h}}_{\text{BLM}}$.

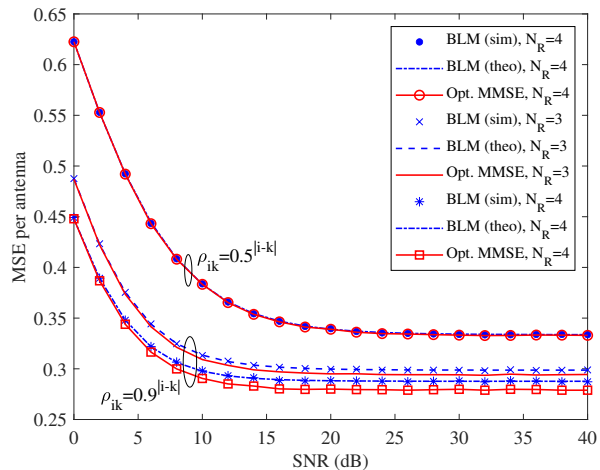


Figure 2. MSE comparison for SIMO case with $N_R = 3, 4$ and exponential channel correlation model.

B. SIMO with $\tau = 1$ and $N_R = 3, 4$

Here, we assume $N_R = 3$ and $N_R = 4$ corresponding to the discussion in Section VI-A. Fig. 2 shows the results using the exponential channel correlation model [36], [37] with $\rho_{ik} = 0.5^{|i-k|}$ or $\rho_{ik} = 0.9^{|i-k|}$, $i, k = 1, \dots, N_R$. We observe that the difference in the MSE performance between $\hat{\mathbf{h}}_{\text{BLM}}$ and $\hat{\mathbf{h}}_{\text{MMSE}}$ is more pronounced at moderate-to-high SNR when both the channel correlation coefficient and N_R grow large. When the channel correlation is low, the performance of the two is similar, as expected according to Theorem 1 (see Remark 5).

C. SIMO with $\tau = 1$ and $\rho_{i,k} = \rho$

Using Theorem 3, we provide simulation results in Fig. 3 for $N_R = 4, 16, 32$ and in Fig. 4 for $N_R = 8, 16, 32, 64$, with $\rho_{i,k} = \rho = 0.9$, for $i \neq k$. In Fig. 3, the curves for $N_R = 4$

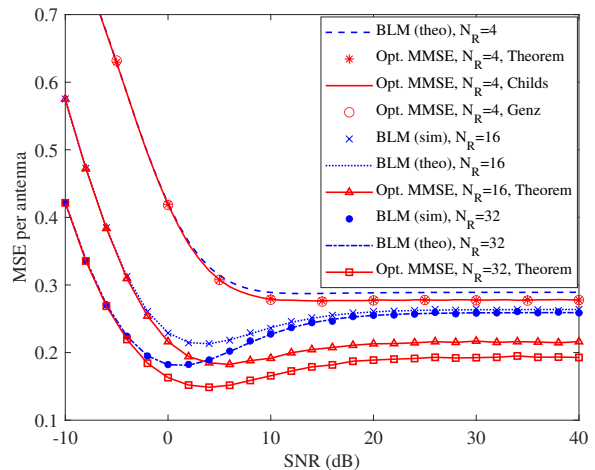


Figure 3. MSE comparison for SIMO case with $N_R = 4, 16, 32$ and the same channel correlation coefficient $\rho = 0.9$ between all antennas.

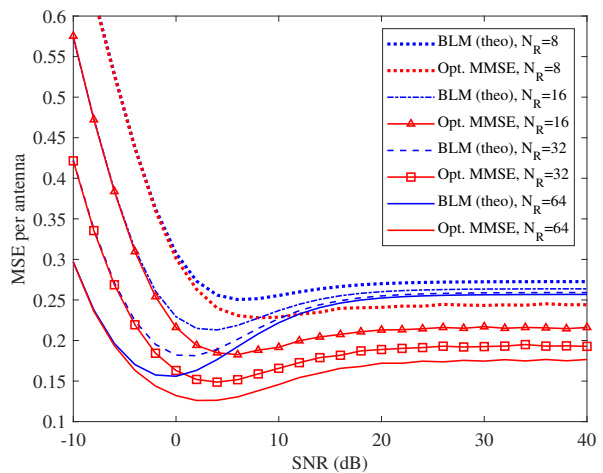


Figure 4. MSE comparison for SIMO case with $N_R = 8, 16, 32, 64$ and the same channel correlation coefficient $\rho = 0.9$ between all antennas.

are obtained using the following three methods: 1) based on Theorem 3, with the corresponding curves labeled “Theorem”; 2) based on the semi-closed-form expression that relies on Appendix A [27], with the corresponding curve labeled “Childs”; and 3) based on (92) along with the algorithm in [31] to obtain the required orthant probabilities via Monte Carlo simulations, with the corresponding curve labeled “Genz”. The results from all three methods coincide, which corroborates the analysis leading to Theorem 3. However, when N_R becomes larger, the semi-closed-form expressions do not exist and the Monte Carlo method [31] also becomes computationally more demanding and less accurate. Consequently, we resort to Theorem 3 to obtain all the curves for the MMSE channel estimate in Fig. 4. We see in Figs. 2–4 that when the channel correlation is high, $\hat{\mathbf{h}}_{\text{MMSE}}$ clearly outperforms $\hat{\mathbf{h}}_{\text{BLM}}$ across a wide range of SNRs, particularly for moderate-to-high SNRs. The per-antenna MSE of $\hat{\mathbf{h}}_{\text{MMSE}}$ improves considerably with N_R at all SNR values, whereas for $\hat{\mathbf{h}}_{\text{BLM}}$, the improvement with N_R

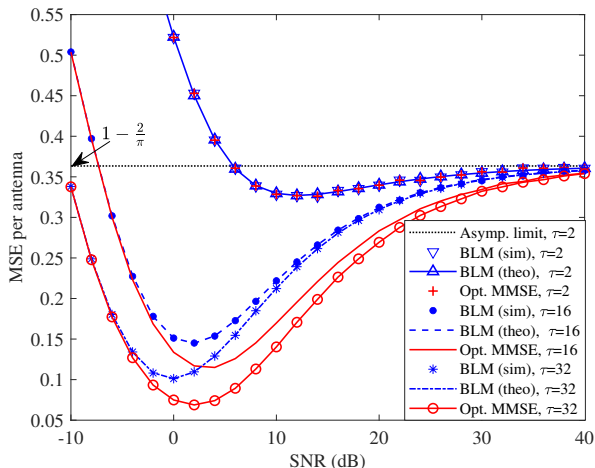


Figure 5. MSE comparison for SISO or SIMO with no receive correlation, $\tau = 2, 16, 32$.

is predominantly observed for relatively low SNRs.

D. Spatially White SIMO or SISO with Multiple Real-Valued Pilots

We investigate the effect of using multiple pilot symbols based on Theorem 4. For the simulations, we use the second column of $\tau \times \tau$ Hadamard matrices as the pilot vector \mathbf{s} . Fig. 5 presents the results for $\tau = 2, 16, 32$. The curves corresponding to $\tau = 2$ corroborate the claim made in Remark 9 and demonstrate the equivalence of the two estimators as well as the equivalence of (73) and (105). It is also visible in Figs. 3–4 that the MSE of both $\hat{\mathbf{h}}_{\text{MMSE}}$ and $\hat{\mathbf{h}}_{\text{BLM}}$ first improves and then deteriorates with the SNR, since it is noise-limited at low SNR and quantization-error-limited at high SNR. For $\tau > 2$, the two estimators exhibit the same asymptotic MSE performance at both low and high SNR. However, significant MSE gains are achievable from non-linear processing for intermediate SNRs. The simulation results validate the high-SNR asymptotic analysis for the case with $\tau = 2$ in (108). Interestingly, the same behavior at high SNR is also observed for $\tau > 2$.

VIII. CONCLUSIONS

In this work, we have investigated optimal MMSE channel estimation for MIMO systems in slow, flat Rayleigh fading channels with one-bit quantization at the receiver. We have developed an explicit framework for the computation of the MMSE estimate, which is related to the orthant probability of the MVN distribution. Leveraging insights gained from this framework, we have fully unraveled the condition for the BLMMSE channel estimator to be MSE optimal. Furthermore, we have derived computationally efficient expressions for the non-linear MMSE estimators under specific assumptions regarding channel correlation or pilot symbols. Our findings reveal that the MSE performance of the low-cost BLMMSE estimator closely approximates that of the MMSE estimator under conditions of low channel correlation, relatively low

SNR, or very high SNR with multiple pilots per transmit antenna. However, with a large number of highly correlated receive antennas or multiple pilot symbols, the MMSE channel estimator yields significant gains over the BLMMSE estimator across a wide range of SNRs. Our results offer unique insights into the one-bit channel estimation problem and provide guidance for applications when N_R or τ is large.

APPENDIX A

THE ORTHANT PROBABILITY IN (36) WITH $L = 4$

Here, we adopt the same notation as in (43). Based on [27], when $L = 4$,

$$\mathcal{P}(\Psi) = \frac{1}{16} + \frac{\arcsin(\psi_{34}) + \sum_{l=3}^4 \arcsin(\psi_{2l})}{8\pi} + \frac{\sum_{k=2}^4 \arcsin(\psi_{1k})}{8\pi} + \frac{\sum_{i=1}^3 \mathcal{J}_i}{4\pi^2}, \quad (109)$$

with

$$\mathcal{J}_1 = \int_0^1 \frac{\psi_{12} \arcsin\left(\frac{d_{34,a} - t^2 d_{34,b}}{\sqrt{(\mu_{23,a} - t^2 \mu_{23,b})(\mu_{24,a} - t^2 \mu_{24,b})}}\right)}{\sqrt{1 - t^2 \psi_{12}^2}} dt, \quad (109a)$$

$$\mathcal{J}_2 = \int_0^1 \frac{\psi_{13} \arcsin\left(\frac{d_{24,a} - t^2 d_{24,b}}{\sqrt{(\mu_{23,a} - t^2 \mu_{23,b})(\mu_{34,a} - t^2 \mu_{34,b})}}\right)}{\sqrt{1 - t^2 \psi_{13}^2}} dt, \quad (109b)$$

$$\mathcal{J}_3 = \int_0^1 \frac{\psi_{14} \arcsin\left(\frac{d_{23,a} - t^2 d_{23,b}}{\sqrt{(\mu_{24,a} - t^2 \mu_{24,b})(\mu_{34,a} - t^2 \mu_{34,b})}}\right)}{\sqrt{1 - t^2 \psi_{14}^2}} dt, \quad (109c)$$

and

$$d_{23,a} = \psi_{23} - \psi_{24}\psi_{34}, \quad (109d)$$

$$d_{24,a} = \psi_{24} - \psi_{23}\psi_{34}, \quad (109e)$$

$$d_{34,a} = \psi_{34} - \psi_{23}\psi_{24}, \quad (109f)$$

$$\mu_{ik,a} = 1 - \psi_{ik}^2 \quad (i < k, i, k = 2, 3, 4), \quad (109g)$$

$$\mu_{ik,b} = \psi_{1i}^2 + \psi_{1k}^2 - 2\psi_{1i}\psi_{1k}\psi_{ik} \quad (i < k, i, k = 2, 3, 4), \quad (109h)$$

$$d_{23,b} = \psi_{12}\psi_{13} + \psi_{14}^2\psi_{23} - \psi_{12}\psi_{14}\psi_{34} - \psi_{13}\psi_{14}\psi_{24}, \quad (109i)$$

$$d_{24,b} = \psi_{12}\psi_{14} + \psi_{13}^2\psi_{24} - \psi_{12}\psi_{13}\psi_{34} - \psi_{13}\psi_{14}\psi_{23}, \quad (109j)$$

$$d_{34,b} = \psi_{13}\psi_{14} + \psi_{12}^2\psi_{34} - \psi_{12}\psi_{14}\psi_{23} - \psi_{12}\psi_{13}\psi_{24}. \quad (109k)$$

APPENDIX B

COMPUTATIONAL CONSIDERATIONS FOR REMARK 4

With a slight abuse of notation, let $\mathbf{q} = [q_1 \ q_2 \ q_3]^T$, with $q_1, q_2, q_3 \in \{\pm 1\}$. Let the pdf $p(\mathbf{u})$ of the real-valued Gaussian random vector $\mathbf{u} = [u_1 \ u_2 \ u_3]^T$ be given by $\mathcal{N}(\mathbf{0}, \Phi)$, with $[\Phi]_{ii} = \sigma_{ui}^2$ and $[\Phi]_{ik} = [\Phi]_{ki} = q_i q_k \phi_{ik} \sigma_{ui} \sigma_{uk}$, $\phi_{ik} \in (-1, 1)$, for $i, k = 1, 2, 3$ and $i \neq k$. Let $\Lambda_{\mathbf{q}} = \text{diag}(\mathbf{q})$. We show through evaluation that $\Lambda_{\mathbf{q}} \int_{\mathbb{R}^3} \mathbf{u} p(\mathbf{u}) d\mathbf{u} / \int_{\mathbb{R}^3} p(\mathbf{u}) d\mathbf{u}$

is not in general linear in \mathbf{q} . The same claim holds when there are more than three elements in \mathbf{q} and \mathbf{u} .

Clearly, $\int_{\mathbb{R}_+^3} p(\mathbf{u})d\mathbf{u} = \mathcal{P}(\Phi)$. Based on (44) and (46),

$$\int_{\mathbb{R}_+^3} p(\mathbf{u})d\mathbf{u} = \frac{1}{8} + \frac{\sum_{i=1}^2 \sum_{k=i+1}^3 q_i q_k \arcsin(\phi_{ik})}{4\pi}. \quad (110)$$

Using the reduction in (32)–(34),

$$\int_{\mathbb{R}_+^3} \mathbf{u}p(\mathbf{u})d\mathbf{u} = \frac{\Phi \left[\int_{\mathbb{R}_+^2} e^{-\frac{\hat{\mathbf{u}}_i^T \Phi_{-i}^{-1} \hat{\mathbf{u}}_i}{2}} d\hat{\mathbf{u}}_i \right]_{i=1}^3}{(2\pi)^{\frac{3}{2}} |\Phi|^{\frac{1}{2}}}, \quad (111)$$

where $\hat{\mathbf{u}}_i$ denotes the 2-dimensional vector derived by deleting the i -th element of \mathbf{u} and Φ_{-i}^{-1} is the 2×2 matrix obtained by deleting the i -th row and column of Φ^{-1} , for $i = 1, 2, 3$. Clearly,

$$\int_{\mathbb{R}_+^2} \exp \left\{ -\frac{1}{2} \hat{\mathbf{u}}_i^T \Phi_{-i}^{-1} \hat{\mathbf{u}}_i \right\} d\hat{\mathbf{u}}_i = 2\pi |\Phi_{-i}|^{\frac{1}{2}} \mathcal{P}(\Phi_{-i}). \quad (112)$$

It can be shown that $|\Phi_{-i}| = |\Phi|/\sigma_{ui}^2$, and from (45),

$$\mathcal{P}(\Phi_{-i}) = \frac{1}{4} + \frac{q_k q_l}{2\pi} \arcsin \left(\frac{\phi_{kl} - \phi_{ik} \phi_{il}}{\sqrt{1 - \phi_{ik}^2} \sqrt{1 - \phi_{il}^2}} \right), \quad (113)$$

for $i, k, l = 1, 2, 3$, $i \neq k$, $i \neq l$, and $k \neq l$. Define $\Lambda_\sigma = \text{diag}[\sigma_{u1} \ \sigma_{u2} \ \sigma_{u3}]^T$. Further capitalizing on the fact that $q_i \in \{\pm 1\}$, for $i = 1, 2, 3$, we obtain

$$\Lambda_{\mathbf{q}} \int_{\mathbb{R}_+^3} \mathbf{u}p(\mathbf{u})d\mathbf{u} = \frac{\Lambda_\sigma}{\sqrt{2\pi}} \begin{bmatrix} 1 & \phi_{12} & \phi_{13} \\ \phi_{12} & 1 & \phi_{23} \\ \phi_{13} & \phi_{23} & 1 \end{bmatrix} \cdot \begin{bmatrix} \frac{q_1}{4} + \frac{q_1 q_2 q_3}{2\pi} \arcsin \left(\frac{\phi_{23} - \phi_{12} \phi_{13}}{\sqrt{1 - \phi_{12}^2} \sqrt{1 - \phi_{13}^2}} \right) \\ \frac{q_2}{4} + \frac{q_1 q_2 q_3}{2\pi} \arcsin \left(\frac{\phi_{13} - \phi_{12} \phi_{23}}{\sqrt{1 - \phi_{12}^2} \sqrt{1 - \phi_{23}^2}} \right) \\ \frac{q_3}{4} + \frac{q_1 q_2 q_3}{2\pi} \arcsin \left(\frac{\phi_{12} - \phi_{13} \phi_{23}}{\sqrt{1 - \phi_{13}^2} \sqrt{1 - \phi_{23}^2}} \right) \end{bmatrix}. \quad (114)$$

From (110) and (114), it is clear that, in general, $\Lambda_{\mathbf{q}} \int_{\mathbb{R}_+^3} \mathbf{u}p(\mathbf{u})d\mathbf{u} / \int_{\mathbb{R}_+^3} p(\mathbf{u})d\mathbf{u}$ is not linear in \mathbf{q} .

APPENDIX C DERIVATION OF (92)

Recall (85)–(88) and (90)–(91). It is clear that $|\mathbf{W}_R| = |\mathbf{W}_I| = 2^{-N_R} |\Omega_b|$. Using (32) and (36), and based on (60), we obtain

$$\begin{aligned} \hat{\mathbf{h}}_{\text{MMSE}} &= s^* \Sigma \mathbf{D}_R \left(\frac{\Lambda_R \int_{\mathbb{R}_+^{N_R}} \mathbf{x} e^{-\frac{\mathbf{x}^T \mathbf{W}_R^{-1} \mathbf{x}}{2}} d\mathbf{x}}{(2\pi)^{\frac{N_R}{2}} |\mathbf{W}_R|^{\frac{1}{2}} \mathcal{P}(\mathbf{W}_R)} \right. \\ &\quad \left. + \frac{j \Lambda_I \int_{\mathbb{R}_+^{N_R}} \mathbf{y} e^{-\frac{\mathbf{y}^T \mathbf{W}_I^{-1} \mathbf{y}}{2}} d\mathbf{y}}{(2\pi)^{\frac{N_R}{2}} |\mathbf{W}_I|^{\frac{1}{2}} \mathcal{P}(\mathbf{W}_I)} \right) \\ &= \frac{s^* \Sigma \mathbf{D}_R}{\pi^{\frac{N_R}{2}} |\Omega_b|^{\frac{1}{2}}} \left(\frac{\Lambda_R \mathbf{W}_R \mathbf{g}_x}{\mathcal{P}(\mathbf{W}_R)} + \frac{j \Lambda_I \mathbf{W}_I \mathbf{g}_y}{\mathcal{P}(\mathbf{W}_I)} \right), \quad (116) \end{aligned}$$

where \mathbf{g}_x (resp. \mathbf{g}_y) is not the same as \mathbf{g}_R (resp. \mathbf{g}_I) in (92). For $k = 1, \dots, N_R$, the k -th element of \mathbf{g}_x is given by

$$g_{x,k} = \int_{\mathbb{R}_+^{N_R-1}} e^{-\frac{1}{2} \mathbf{x}_{-k}^T \mathbf{W}_{x,k}^{-1} \mathbf{x}_{-k}} d\mathbf{x}_{-k} \quad (117)$$

$$= (2\pi)^{\frac{N_R-1}{2}} |\mathbf{W}_{x,k}|^{\frac{1}{2}} \mathcal{P}(\mathbf{W}_{x,k}), \quad (118)$$

with $\mathbf{x}_{-k} = [x_1 \ \dots \ x_{k-1} \ x_{k+1} \ \dots \ x_{N_R}]^T$. Similarly,

$$\mathbf{g}_y = \left[(2\pi)^{\frac{N_R-1}{2}} |\mathbf{W}_{y,k}|^{\frac{1}{2}} \mathcal{P}(\mathbf{W}_{y,k}) \right]_{k=1}^{N_R}. \quad (119)$$

From (39), we obtain $|\mathbf{D}_{R,-k}^{-1}| = \frac{|\Omega_b|}{|s|^2 + \sigma^2}$, and thus from (90)–(91), for $k = 1, \dots, N_R$, we have

$$|\mathbf{W}_{x,k}| = |\mathbf{W}_{y,k}| = \frac{2^{-(N_R-1)} |\Omega_b|}{|s|^2 + \sigma^2}. \quad (120)$$

Based on the above steps, (116) is further simplified to (92).

APPENDIX D PROOF OF THEOREM 3

Proof: Recall (85)–(88) and the starting point (92). Each off-diagonal element of \mathbf{W}_R (resp. \mathbf{W}_I) is affected by two different elements from \mathbf{r}_R (resp. \mathbf{r}_I). Specifically, the (i, k) -th element of the standardized version of \mathbf{W}_R is given by $\left(r_{R,i} \sqrt{\frac{|s|^2 \rho}{|s|^2 + \sigma^2}} \right) \left(r_{R,k} \sqrt{\frac{|s|^2 \rho}{|s|^2 + \sigma^2}} \right)$, for $i, k = 1, \dots, N_R$ and $i \neq k$. Based on Lemma [30, p. 192] and using (44), $\mathcal{P}(\mathbf{W}_R)$ is given by (96). Similarly, $\mathcal{P}(\mathbf{W}_I)$ is obtained.

By assumption, Σ is a standardized circulant matrix with all the off-diagonal elements equal to ρ . The inverse of Σ is also a circulant matrix [40] given by:

$$\Sigma^{-1} = \frac{[1 + (N_R - 2)\rho] \Sigma_{\text{inv,circ}}}{1 + (N_R - 2)\rho - (N_R - 1)\rho^2}, \quad (121)$$

where $\Sigma_{\text{inv,circ}}$ is a standardized circulant matrix whose off-diagonal elements are equal to $\left(-\frac{\rho}{1 + (N_R - 2)\rho} \right)$. Clearly, here Ω_b and its inverse \mathbf{D}_R are also circulant matrices. Consider $\mathbf{D}_{R,-k}$, for $k = 1, \dots, N_R$. Using (121), the $(N_R - 1) \times (N_R - 1)$ circulant matrix $\mathbf{D}_{R,-k}^{-1}$ is given by

$$\mathbf{D}_{R,-k}^{-1} = \frac{((|s|^2 + \sigma^2)^2 - |s|^4 \rho^2) \mathbf{D}_{\text{inv,circ}}}{|s|^2 + \sigma^2}, \quad (122)$$

where $\mathbf{D}_{\text{inv,circ}}$ is a standardized circulant matrix with off-diagonal elements given by $\frac{\rho |s|^2}{[|s|^2(1+\rho)] + \sigma^2}$. From (122) and (90), the (i, l) -th element of the standardized version of $\mathbf{W}_{x,k}$ is given by $\left(r_{R,i} \sqrt{\frac{|s|^2 \rho}{|s|^2(1+\rho) + \sigma^2}} \right) \left(r_{R,l} \sqrt{\frac{|s|^2 \rho}{|s|^2(1+\rho) + \sigma^2}} \right)$, for $i, l = 1, \dots, N_R$, $i \neq l$, $i \neq k$, and $l \neq k$. Invoke the results in [30] again to obtain $\mathcal{P}(\mathbf{W}_{x,k})$ as given by (97), and similarly obtain $\mathcal{P}(\mathbf{W}_{y,k})$, $k = 1, \dots, N_R$. ■

APPENDIX E PROOF OF THEOREM 4

Proof: Recall (99) with $\mathbf{D}_I = \mathbf{0}$, so that (60) holds. Also recall (102) and (103)–(104). Following similar steps to those leading to (116) in Appendix C, we have

$$\hat{\mathbf{h}}_{\text{MMSE}} = \frac{s^T \mathbf{D}_R}{(2\pi)^{\frac{N_R}{2}}} \left(\frac{\Lambda_R \mathbf{W}_A \mathbf{g}_A}{|\mathbf{W}_A|^{\frac{1}{2}} \mathcal{P}(\mathbf{W}_A)} + \frac{j \Lambda_I \mathbf{W}_B \mathbf{g}_B}{|\mathbf{W}_B|^{\frac{1}{2}} \mathcal{P}(\mathbf{W}_B)} \right), \quad (123)$$

where, for $k = 1, \dots, \tau$, the k -th element of \mathbf{g}_A is given by

$$g_{A,k} = \int_{\mathbb{R}_+^{\tau-1}} e^{-\frac{\tilde{\mathbf{x}}_{-k}^T \mathbf{W}_{A,k}^{-1} \tilde{\mathbf{x}}_{-k}}{2}} d\tilde{\mathbf{x}}_{-k} \quad (124)$$

$$= (2\pi)^{\frac{\tau-1}{2}} |\mathbf{W}_{A,k}|^{\frac{1}{2}} \mathcal{P}(\mathbf{W}_{A,k}), \quad (125)$$

and $\tilde{\mathbf{x}}_{-k} = [x_1 \dots x_{k-1} \ x_{k+1} \dots x_\tau]^T$. Similarly, we have $\mathbf{g}_B = \left[(2\pi)^{\frac{\tau-1}{2}} |\mathbf{W}_{B,k}|^{\frac{1}{2}} \mathcal{P}(\mathbf{W}_{B,k}) \right]_{k=1}^\tau$. According to [30, p. 192], $\mathcal{P}(\mathbf{W}_A)$ is given by (106), and $\mathcal{P}(\mathbf{W}_B)$ is similarly obtained. Using (101) and (103)–(104), again based on [30, p. 192], $\mathcal{P}(\mathbf{W}_{A,k})$ is shown to be given by (107) and $\mathcal{P}(\mathbf{W}_{B,k})$ is similarly derived. From [34, p. 475], for a non-singular $L \times L$ matrix \mathbf{E} and L -dimensional vectors \mathbf{e}_a and \mathbf{e}_b , $|\mathbf{E} + \mathbf{e}_a \mathbf{e}_b^T| = |\mathbf{E}| (1 + \mathbf{e}_b^T \mathbf{E}^{-1} \mathbf{e}_a)$. Apply this identity to obtain $|\mathbf{W}_A| = |\mathbf{W}_B| = \left(\frac{\sigma^2}{2}\right)^\tau \left(1 + \frac{\mathbf{s}^T \mathbf{s}}{\sigma^2}\right)$ and $|\mathbf{W}_{A,k}| = |\mathbf{W}_{B,k}| = \left(\frac{\sigma^2}{2}\right)^{\tau-1} \left(\frac{\mathbf{s}_{-k}^T \mathbf{s}_{-k} + \sigma^2}{\sigma^2 + \sigma^2}\right)$. Inserting the above results into (123), we obtain (105) after some algebraic manipulations. ■

REFERENCES

- [1] E. Larsson, O. Edfors, F. Tufvesson, and T. Marzetta, "Massive MIMO for next generation wireless systems," *IEEE Commun. Mag.*, vol. 52, no. 2, pp. 186–195, 2014.
- [2] F. Rusek, et al., "Scaling up MIMO: Opportunities and challenges with very large arrays," *IEEE Signal Process. Mag.*, vol. 30, no. 1, pp. 40–60, 2013.
- [3] E. Björnson, J. Hoydis, and L. Sanguinetti, "Massive MIMO networks: Spectral, energy, and hardware efficiency," *Found. and Trends Signal Process.*, vol. 11, no. 3–4, pp. 154–655, 2017.
- [4] N. Rajatheva, I. Atzeni, E. Björnson et al., "White paper on broadband connectivity in 6G," 2020. [Online]. Available: <http://jultika.oulu.fi/files/isbn9789526226798.pdf>
- [5] R. Walden, "Analog-to-digital converter survey and analysis," *IEEE J. Sel. Areas Commun.*, vol. 17, no. 4, pp. 539–550, 1999.
- [6] J. Mo and R. Heath, Jr., "Capacity analysis of one-bit quantized MIMO systems with transmitter channel state information," *IEEE Trans. Signal Process.*, vol. 63, no. 20, pp. 5498–5512, 2015.
- [7] Y. Li, C. Tao, G. Seco-Granados, A. Mezghani, A. L. Swindlehurst, and L. Liu, "Channel estimation and performance analysis of one-bit massive MIMO systems," *IEEE Trans. Signal Process.*, vol. 65, no. 15, pp. 4075–4089, 2017.
- [8] I. Atzeni, A. Tölili, and G. Durisi, "Low-resolution massive MIMO under hardware power consumption constraints," in *Proc. Asilomar Conf. Signals, Syst., and Comput. (ASILOMAR)*, 2021.
- [9] C. Mollén, J. Choi, E. G. Larsson, and R. W. Heath, "Uplink performance of wideband massive MIMO with one-bit ADCs," *IEEE Trans. Wireless Commun.*, vol. 16, no. 1, pp. 87–100, 2017.
- [10] S. Jacobsson, G. Durisi, M. Coldrey, U. Gustavsson, and C. Studer, "Throughput analysis of massive MIMO uplink with low-resolution ADCs," *IEEE Trans. Wireless Commun.*, vol. 16, no. 6, pp. 4038–4051, 2017.
- [11] J. Mo, P. Schniter, and R. W. Heath, Jr., "Channel estimation in broadband millimeter wave MIMO systems with few-bit ADCs," *IEEE Trans. Signal Process.*, vol. 66, no. 5, pp. 1141–1154, 2018.
- [12] N. Bernardo, J. Zhu, Y. C. Eldar, and J. Evans, "Capacity bounds for one-bit MIMO Gaussian channels with analog combining," *IEEE Trans. Commun.*, vol. 70, no. 11, pp. 7224–7239, 2022.
- [13] M. Shao and W.-K. Ma, "Divide and conquer: One-bit MIMO-OFDM detection by inexact expectation maximization," in *Proc. IEEE Int. Conf. Acoust., Speech, and Signal Process. (ICASSP)*, 2021.
- [14] J. Choi, J. Mo, and R. W. Heath Jr., "Near maximum-likelihood detector and channel estimator for uplink multiuser massive MIMO systems with one-bit ADCs," *IEEE Trans. Commun.*, vol. 64, no. 5, pp. 2005–2018, 2016.
- [15] S. Rao, A. Mezghani, and A. L. Swindlehurst, "Channel estimation in one-bit massive MIMO systems: Angular versus unstructured models," *IEEE J. Sel. Topics Signal Process.*, vol. 13, no. 5, pp. 1017–1031, 2019.
- [16] M. S. Stein, S. Bar, J. A. Nossek, and J. Tabrikian, "Performance analysis for channel estimation with 1-bit ADC and unknown quantization threshold," *IEEE Trans. Signal Process.*, vol. 66, no. 10, pp. 2557–2571, 2018.
- [17] I. Atzeni and A. Tölili, "Channel estimation and data detection analysis of massive MIMO with 1-bit ADCs," *IEEE Trans. Wireless Commun.*, vol. 21, no. 6, pp. 3850–3867, 2022.
- [18] I. Atzeni and A. Tölili, "Uplink data detection analysis of 1-bit quantized massive MIMO," in *Proc. IEEE Int. Workshop Signal Process. Adv. in Wireless Commun. (SPAWC)*, 2021.
- [19] B. Fesl, M. Koller, and W. Utschick, "On the mean square error optimal estimator in one-bit quantized systems," *IEEE Trans. Signal Process.*, vol. 71, pp. 1968–1980, 2023.
- [20] J. J. Bussgang, "Crosscorrelation functions of amplitude-distorted Gaussian signals," *Res. Lab. Electron., MIT, Cambridge, MA, U.S.A.*, 1952.
- [21] G. Jacovitti and A. Neri, "Estimation of the autocorrelation function of complex Gaussian stationary processes by amplitude clipped signals," *IEEE Trans. Inf. Theory*, vol. 40, no. 1, pp. 239–245, 1994.
- [22] A. K. Saxena, I. Fijalkow, and A. L. Swindlehurst, "Analysis of one-bit quantized precoding for the multiuser massive MIMO downlink," *IEEE Trans. Signal Process.*, vol. 65, no. 17, pp. 4624–4634, 2017.
- [23] S. Jacobsson, G. Durisi, M. Coldrey, and C. Studer, "Linear precoding with low-resolution DACs for massive MU-MIMO-OFDM downlink," *IEEE Trans. Wireless Commun.*, vol. 18, no. 3, pp. 1595–1609, 2019.
- [24] S. M. Kay, *Fundamentals of Statistical Signal Processing: Estimation Theory*. Prentice-Hall, 1993.
- [25] R. E. Curry, *Estimation and Control with Quantized Measurements*. The MIT Press, 1970.
- [26] I. G. Abrahamson, "Orthant probabilities of the quadrivariate normal distribution," *Ann. Math. Statist.*, vol. 35, no. 4, pp. 1685–1703, 1964.
- [27] D. R. Childs, "Reduction of the multivariate normal integral to characteristic form," *Biometrika*, vol. 54, no. 1–2, pp. 293–300, 1967.
- [28] R. L. Plackett, "A reduction formula for normal multivariate integrals," *Biometrika*, vol. 41, no. 3–4, pp. 351–360, 1954.
- [29] H.-J. Sun, "A general reduction method for n -variate normal orthant probability," *Comm. Statist. Theory Methods*, vol. 17, no. 11, pp. 3913–3921, 1988.
- [30] Y. L. Tong, *The Multivariate Normal Distribution*. Springer-Verlag, 1990.
- [31] A. Genz, "Numerical computation of multivariate normal probabilities," *J. Comput. Graphical Statist.*, vol. 1, no. 2, pp. 141–149, 1992.
- [32] D. M. Keenan, "A time series analysis of binary data," *J. Amer. Statist. Assoc.*, vol. 77, no. 380, pp. 816–821, 1982.
- [33] M. Sinn and K. Keller, "Covariances of zero crossings in Gaussian processes," *Theory Probab. Appl.*, vol. 55, no. 3, pp. 485–504, 2011.
- [34] C. D. Meyer, *Matrix Analysis and Applied Linear Algebra*. SIAM, 2000.
- [35] R. A. Johnson and D. W. Wichern, *Applied Multivariate Statistical Analysis*. Pearson Education Inc., 2007.
- [36] V. Aalo, "Performance of maximal-ratio diversity systems in a correlated Nakagami-fading environment," *IEEE Trans. Commun.*, vol. 43, no. 8, pp. 2360–2369, 1995.
- [37] M. Chiani, M. Z. Win, and A. Zanella, "On the capacity of spatially correlated MIMO Rayleigh-fading channels," *IEEE Trans. Inf. Theory*, vol. 49, no. 10, pp. 2363–2371, 2003.
- [38] A. Abdi and M. Kaveh, "A space-time correlation model for multielement antenna systems in mobile fading channels," *IEEE J. Sel. Areas Commun.*, vol. 20, no. 3, pp. 550–560, 2002.
- [39] W. C. Jakes, *Microwave Mobile Communications*. Wiley-IEEE Press, 1974.
- [40] R. M. Gray, "Toeplitz and Circulant Matrices: A Review," *Found. and Trends Commun. and Inf. Theory*, vol. 2, no. 3, pp. 155–239, 2006.